

# 1 Impacts of elevated anthropogenic emissions on physicochemical 2 characteristics of BC-containing particles over the Tibetan Plateau

3 Jinbo Wang<sup>1,2</sup>, Jiaping Wang<sup>1,2,3\*</sup>, Yuxuan Zhang<sup>1,2,3,4</sup>, Tengyu Liu<sup>1,2,3</sup>, Xuguang Chi<sup>1,2,3</sup>, Xin Huang<sup>1,2</sup>,  
4 Dafeng Ge<sup>1,2</sup>, Shiyi Lai<sup>1,2</sup>, Caijun Zhu<sup>1,2</sup>, Lei Wang<sup>1,2,3</sup>, Qiaozhi Zha<sup>1,2,3</sup>, Ximeng Qi<sup>1,2,3</sup>, Wei Nie<sup>1,2,3</sup>,  
5 Congbin Fu<sup>1,2,3</sup> and Aijun Ding<sup>1,2,3</sup>

6 <sup>1</sup>Joint International Research Laboratory of Atmospheric and Earth System Sciences, School of Atmospheric Sciences, Nanjing  
7 University, Nanjing, 210023, China.

8 <sup>2</sup>Jiangsu Provincial Collaborative Innovation Center of Climate Change, Nanjing, 210023, China.

9 <sup>3</sup>National Observation and Research Station for Atmospheric Processes and Environmental Change in Yangtze River Delta,  
10 Nanjing, 210023, China.

11 <sup>4</sup>Key Laboratory of Atmospheric Environment and Extreme Meteorology, Institute of Atmospheric Physics, Chinese Academy  
12 of Sciences, Beijing, 100029, China.

13 *Correspondence to:* Jiaping Wang (wangjp@nju.edu.cn)

## 14 **Abstract.**

15 Black carbon (BC) in the Tibetan Plateau (TP) region has distinct climate effect, which strongly depends on its mixing state.  
16 The aging processes of BC in TP are subject to emissions from various regions, resulting in considerable variability of its  
17 mixing state and physicochemical properties. However, the mechanism and magnitude of this effect are not yet clear. In this  
18 study, field observations on physicochemical properties of BC-containing particles ( $PM_{BC}$ ) were conducted in the northeast  
19 (Xihai) and southeast (Lulang) regions of the TP to investigate the impacts of transported emissions from lower-altitude areas  
20 on BC characteristics in the TP. Large spatial discrepancies were found in the chemical composition of  $PM_{BC}$ . Both sites  
21 showed higher concentrations of  $PM_{BC}$  when they were affected by transported airmasses outside the TP, but with diverse  
22 chemical composition. Source apportionment for organic aerosol (OA) suggested that primary OA in the northeastern TP was  
23 attributed to hydrocarbon OA (HOA) from anthropogenic emissions, while it was dominated by biomass burning OA (BBOA)  
24 in the southeastern TP. Regarding secondary aerosol, a marked enhancement in nitrate fraction was observed on aged BC  
25 coating in Xihai when the airmasses were brought by updrafts and easterly winds from lower-altitude areas. With the  
26 development of boundary layer, the enhanced turbulent mixing promoted the elevation of anthropogenic pollutants. In contrast  
27 to Xihai, the thickly coated BC in Lulang was mainly caused by elevation and transportation of biomass burning plume from  
28 the South Asia, showing a large contribution of secondary organic aerosol (SOA). The distinct transported emissions lead to  
29 substantial variations of both chemical composition and light absorption ability of BC across the TP. The thicker coating and  
30 higher mass absorption cross-section (MAC) of  $PM_{BC}$  in airmasses elevated from lower-altitude regions reveals the promoted  
31 BC aging processes and their impacts on the mixing state and light absorption of BC in TP. These findings emphasize the  
32 vulnerability of plateau regions to influences of elevated emissions, leading to significant changes in BC concentration, mixing

33 states and light absorption across the TP, which needs to be considered in the evaluation of BC radiative effects for the TP  
34 region.

## 35 **1 Introduction**

36 The Tibetan Plateau (TP) is the largest plateau of the world, covering approximately 2.5 million km<sup>2</sup>. Its average altitude  
37 exceeds 4,000 m and its glaciers cover an area of over 100,000 km<sup>2</sup> (Yao et al., 2012a). As the third pole, the TP plays a crucial  
38 role in the Asian monsoon systems, the hydrological cycle and global climate (Duan and Wu, 2005; Wu et al., 2007; Wu et  
39 al., 2015). Pollutants in TP and its surrounding region affect significantly the ecological environment of TP. They result in  
40 increased air temperature (Gustafsson and Ramanathan, 2016), changes in cloud properties (Hua et al., 2020; Lai et al., 2024),  
41 glacier retreat (Kang et al., 2010; Kang et al., 2019; Xu et al., 2009; Yao et al., 2012b), anomalies in the hydrological cycle  
42 (Luo et al., 2020; Yang et al., 2014; Menon et al., 2002) and the Asian monsoon (Meehl et al., 2008).

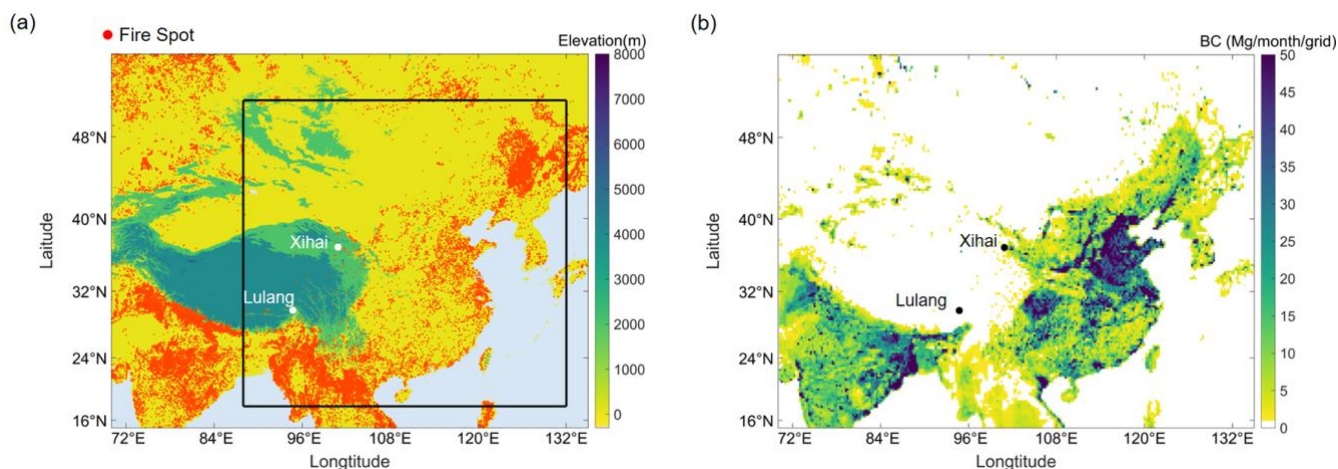
43 Black carbon (BC) is one of the most important aerosol species affecting climate, glaciers and hydrology in TP  
44 (Ramanathan et al., 2005; Xu et al., 2009; Yang et al., 2022) because of distinct climate effect (Bond et al., 2013). It is generated  
45 by the incomplete combustion of fossil fuels and biomass and is also known as refractory BC (rBC). BC influences the climate  
46 directly because it can absorb short-wave radiation. The climate forcing of BC is highly dependent on its mixing state. BC can  
47 be coated with non-refractory aerosol like organics, nitrate (NO<sub>3</sub><sup>-</sup>), sulphate (SO<sub>4</sub><sup>2-</sup>) through condensation or coagulation, and  
48 turns from externally mixed to internally mixed structure. The mass absorption cross-section (MAC) of BC-containing particles  
49 (PM<sub>BC</sub>) can be affected by non-refractory components coated on BC (Cai et al., 2022; Cheng et al., 2016; Gao et al., 2021) via  
50 the “lensing effect” (Lack and Cappa, 2010), causing the change in radiative properties of BC. The cloud microphysical  
51 properties may also be altered when PM<sub>BC</sub> are coated with hydrophilic materials and activated into cloud condensation nuclei  
52 (CCN), which influences climate indirectly (Bond et al., 2013; Dusek et al., 2006; Henning et al., 2010; Liu et al., 2017;  
53 Schnaiter et al., 2005; Wang et al., 2023).

54 Previous studies have shown that BC has a remarkable direct radiative effect in TP (Zhu et al., 2017; Sun et al., 2016;  
55 Zhao et al., 2017; Liu et al., 2021). The radiative effects of BC are not only influenced by its concentration but also by its  
56 mixing state. In recent years, there has been an increasing number of field measurements of BC in TP. It is reported that BC  
57 concentration can still reach high level occasionally in TP under certain meteorological and synoptic condition (Babu et al.,  
58 2011; Zhu et al., 2016; Zhao et al., 2017). Observations on BC mixing states demonstrated that BC is mainly internally mixed  
59 (Yuan et al., 2019), and the BC coating enhances the MAC of BC in TP (Wang et al., 2017; Wang et al., 2018; Chen et al.,  
60 2019; Tan et al., 2021). BC can be transported over long distance with wildfire plumes (Huang et al., 2023; Zheng et al., 2020).  
61 Some regions of TP may be affected by biomass burning (BB) from lower-altitude area (Cao et al., 2010; Zhang et al., 2015;  
62 Cong et al., 2015). External transport can raise BC concentration and affect its morphology and mixing state in TP (Tan et al.,  
63 2021; Chen et al., 2023). However, research on how emissions from various sources affect the chemical composition of PM<sub>BC</sub>  
64 in TP is scarce. Therefore, we conducted field observations of the physicochemical characteristics of PM<sub>BC</sub> at two typical sites  
65 in TP. The objective of this study is to investigate the impacts of various pollutant emissions and the subsequent regional  
66 transport, particularly those from anthropogenic activities from low-altitude regions, on the mixing state and chemical  
67 composition of PM<sub>BC</sub> in TP.

## 68 2. Materials and Methods

### 69 2.1 Site Description

70 Field measurements were conducted at two observation stations in TP (Fig. 1). The station of northeast TP is located in  
71 Xihai town (~ 3100 m a.s.l, 36°56' N, 100°54' E). The station of southeast TP is the South-East Tibetan plateau Station for  
72 integrated observation and research of alpine environment, located in Lulang (~3200 m a.s.l, 29°44' N, 94°44' E). The field  
73 campaign was conducted from April 2 to May 16, 2021 in Lulang and from June 3 to June 23, 2021 in Xihai. Both stations are  
74 typical high-altitude sites of mountainous areas (Fig. 1a) but potentially influenced by distinct emission sources. There is more  
75 wildfire around Lulang (Fig. 1a), but Xihai is close to the northwest region of China which may largely affected by the  
76 anthropogenic emissions (Fig. 1b).



77

78 **Figure 1: The maps showing the (a) topographic height and (b) the anthropogenic emissions of BC in the two measurement sites**  
79 **(Xihai, Lulang) and the surrounding region. The red spots represent the wild fire spots during the field measurement period, and**  
80 **the black-line square represents the simulated domain.**

### 81 2.2 Instrumentation

82 The Soot Particle Aerosol Mass Spectrometer (SP-AMS, Aerodyne Inc., USA) was used to measure rBC and non-  
83 refractory materials coated on rBC (NR-PM<sub>BC</sub>) (Onasch et al., 2012). The tungsten vaporizer was removed and the intracavity  
84 infrared laser vaporizer was reserved to exclusively measure PM<sub>BC</sub>. After adjusting the SP-AMS to the laser-only  
85 configuration, only PM<sub>BC</sub> can be volatilized via absorbing laser. We collected V-mode data due to its high sensitivity (Decarlo  
86 et al., 2006). The total flow rate through the inlet was maintained at ~3L min<sup>-1</sup>. A PM<sub>2.5</sub> cyclone was used in the front of the  
87 inlet (URG Corp., USA), and only particles in the size range of 50-1000 nm can be focused by the lens of inlet system. The  
88 bounce effect of aerosol was eliminated because the tungsten vaporizer was removed, so the usual collection efficiency (CE)  
89 is not applicable (Docherty et al., 2013; Drewnick et al., 2005). The overlap of particle beam and laser beam determined the  
90 CE of SP-AMS with laser-only configuration. The new CE was acquired by intercomparison of rBC concentration measured  
91 using SP2 and SP-AMS (Willis et al., 2014; Massoli et al., 2015), and was nearly 1 during this campaign.

92 SP-AMS data was processed by the standard Time-of-Flight AMS data analysis software packages (SQUIRREL version  
93 v1.60P and PIKA v1.20P). Ionization efficiency (IE) calibration was done shortly before removing the tungsten vaporizer. The  
94 mass-based calibration method was used to obtain IE values by sampling the 300 nm dried pure ammonium nitrate particles  
95 into SP-AMS. The 300 nm particles were selected with a differential mobility analyzer (DMA, model 3081, TSI Inc., USA).  
96 The relative IE (RIE) for organic aerosol (OA) and  $\text{SO}_4^{2-}$  was 1.4 and 1.2, which was consistent to the RIE reported in a  
97 previous work (Canagaratna et al., 2007). The RIE for rBC was calibrated by sampling monodispersed 300 nm Regal Black  
98 particles into SP-AMS. The detection limit was calculated based on the method in Decarlo et al (2006), and the detection limit  
99 of ammonium was higher, so the concentration of ammonium was estimated by ionic equilibrium. OA measured by the SP-  
100 AMS were subdivided into factors with different characteristics and sources based on positive matrix factorization (PMF)  
101 results. The PMF Evaluation Tool version 3.04A was used to perform PMF analysis on the high-resolution organic mass  
102 spectra (Ulbrich et al., 2009; Zhang et al., 2005b; Zhang et al., 2011). Only ions with charge-to-mass ratio below approximately  
103 115 were considered in the PMF analysis.

104 The meteorological parameters, aerosol optical properties and gaseous pollutants were also measured simultaneously.  
105 Ozone ( $\text{O}_3$ ), carbon monoxide (CO), nitric oxide (NO), nitrogen oxides ( $\text{NO}_x$ ) and sulfur dioxide ( $\text{SO}_2$ ) were measured using  
106 online analyzers (Teledyne API Inc., USA). The photoacoustic extinctions (PAX, Droplet Measurement Technologies Inc.,  
107 USA) measured light absorption coefficients. Temperature, relative humidity (RH) and other meteorological parameters were  
108 monitored by meteorological sensors (WXT530, Vaisala Inc., Finland).

### 109 **2.3 Model configuration**

110 In this study, we conducted regional chemical transport modeling using the Weather Research and Forecasting model  
111 coupled with Chemistry (WRF-Chem, version 3.7.1). This model encompasses a broad spectrum of physical and chemical  
112 processes, addressing the emission and deposition of pollutants, advection, diffusion, gaseous and aqueous chemical  
113 transformations, as well as aerosol chemistry and dynamics (Grell et al., 2005). The model domain was centered at 35°N and  
114 110°E with a grid resolution of 20 km, covering the northeastern Tibetan Plateau. The vertical structure of the model comprised  
115 30 layers extending from the surface to the top pressure of 50 hPa. The simulation was conducted for the longer period  
116 including the times of whole campaign from 3 June to 11 June 2021. To establish accurate initial and boundary conditions for  
117 meteorological fields, we updated the model using 6-hourly  $1^\circ \times 1^\circ$  National Centers for Environmental Prediction (NCEP)  
118 global final analysis (FNL) data. In our pursuit of well capturing the meteorological fields, we assimilated National Centers  
119 for Environmental Prediction (NCEP) Automated Data Processing (ADP) operation global surface observation and global  
120 upper air observational weather data. This assimilation process utilized default nudging coefficients for wind, temperature, and  
121 moisture.

122 The Yonsei University planetary boundary layer (YSU PBL) scheme was used to parameterize boundary layer processes  
123 (Hong et al., 2006). Other essential physical parameterization options included the unified Noah land surface model (Ek et al.,  
124 2003), the Lin microphysics scheme (Lin et al., 1983), and the Grell-Freitas cumulus parameterization scheme (Grell and

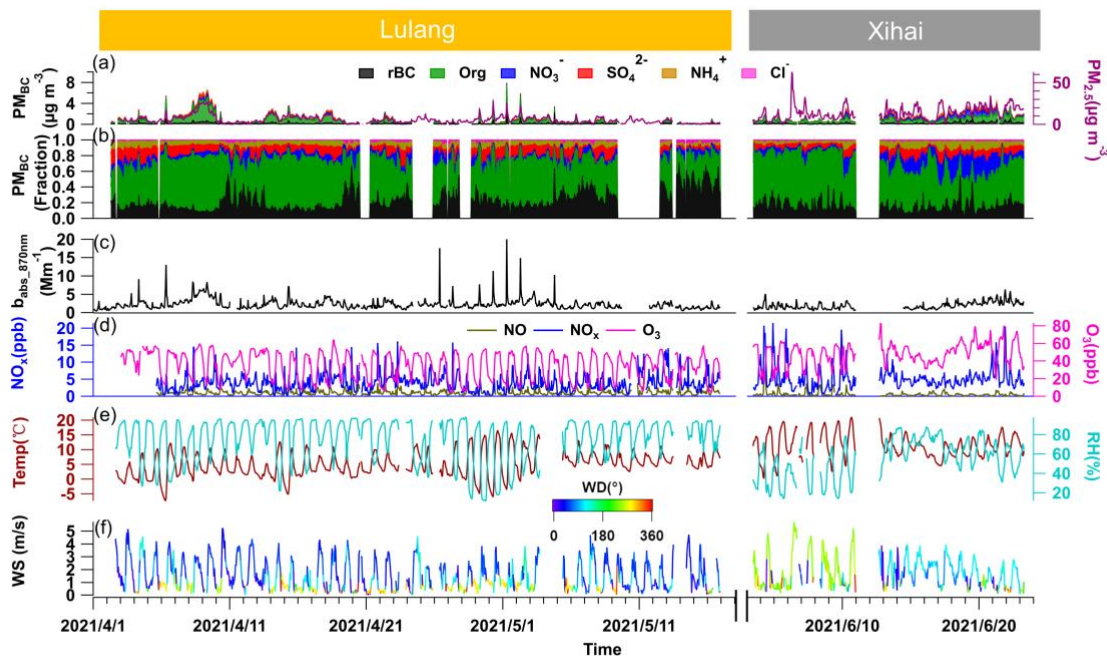
125 Freitas, 2014). For representing atmospheric chemistry numerically, we utilized the Carbon-Bond Mechanism version Z  
126 photochemical mechanism along with the Model for Simulating Aerosol Interactions and Chemistry aerosol module (Zaveri  
127 and Peters, 1999; Zaveri et al., 2008). Both natural and anthropogenic emissions were considered in this regional WRF-Chem  
128 modeling study. Anthropogenic emissions were derived from the Multi-resolution Emission Inventory for China (MEIC),  
129 which includes emissions from power plants, residential combustion, industrial processes, on-road mobile sources, and  
130 agricultural activities (Li et al., 2017). Biogenic emissions were calculated online using the Model of Emissions of Gases and  
131 Aerosols from Nature (MEGAN), encompassing more than 20 biogenic species (Guenther et al., 2006).

132 A comprehensive overview of the model configuration can be referenced in earlier investigations (Huang et al., 2016;  
133 Huang et al., 2018). Additionally, key configurations and validation for the WRF-Chem regional modeling are shown by Table  
134 S1 and Fig. S1.

#### 135 **2.4 Other materials**

136 The transport and emission condition were considered to investigate their impacts on BC physical and chemical properties.  
137 The Hybrid Single-Particulate Lagrangian Integrated Trajectory (HYSPLIT) model was used to calculate and cluster 72 h  
138 backward trajectories (Stein et al., 2015; Xu et al., 2018). The starting points of the simulation were Xihai and Lulang, and  
139 particles were released at a height of 1000 m above the ground level. The backward trajectories were calculated every hour  
140 during the field campaign. The Fire Inventory from NCAR (FINN) was adopted to estimate daily open BB emissions with  
141 high spatial resolution (1 km) during the campaign (Wiedinmyer et al., 2006; Wiedinmyer et al., 2011; Wiedinmyer et al.,  
142 2023), and the anthropogenic emissions of major pollutants was estimated by MIX-Asia emission inventory (Li et al., 2017).

143 Besides, the optical properties of  $PM_{BC}$  were investigated based on the widely-used core-shell Mie model (Bohren and  
144 Huffman, 1983; Virkkula, 2021). MAC and  $E_{abs}$  of  $PM_{BC}$  were calculated following the algorithm developed by Mätzler (2002).  
145 The refractive index was  $1.95 - 0.79i$  for rBC (Bond and Bergstrom, 2006), and was  $1.52 - 10^{-6}i$  for BC coating (Pitchford et  
146 al., 2007) at 550 nm wavelength. The calculated optical properties of  $PM_{BC}$  in  $PM_1$  were validated by good agreements to  
147 observed results of BC in  $PM_{2.5}$  (Fig. S2).



150

151 **Figure 2: The time series of (a) mass concentrations of particulate matters (PM<sub>2.5</sub>), refractory black carbon (rBC), organics (Org),**  
 152 **nitrate (NO<sub>3</sub><sup>-</sup>), sulphate (SO<sub>4</sub><sup>2-</sup>), ammonium (NH<sub>4</sub><sup>+</sup>) and chloride (Cl<sup>-</sup>) in PM<sub>BC</sub>, (b) mass fraction of different species in PM<sub>BC</sub>, (c)**  
 153 **aerosol light absorption coefficients (b<sub>abs</sub>) at 870 nm wavelength, (d) gaseous pollutants including nitric oxide (NO), nitrogen oxide**  
 154 **(NO<sub>2</sub>) and ozone (O<sub>3</sub>), (e) air temperature (Temp) and relative humidity (RH), (f) wind direction (WD) and wind speed (WS).**

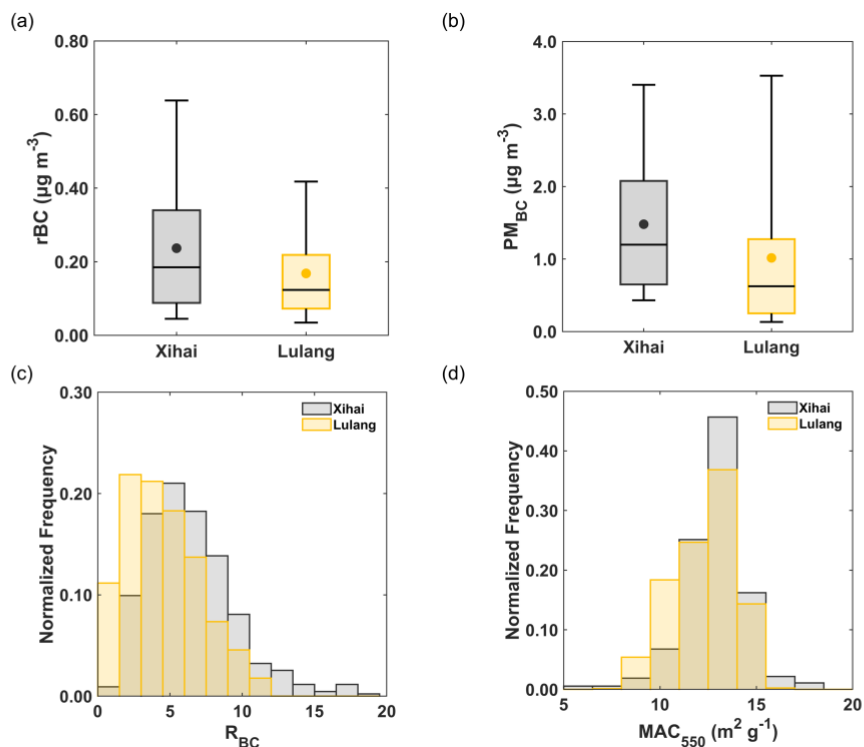
155 Fig. 2 presents the overall condition during the campaign. The mass concentration of rBC shows large temporal variation  
 156 at both sites, with ranges of 0.02–1.28 µg m<sup>-3</sup> in Xihai and 0.02–2.22 µg m<sup>-3</sup> in Lulang. PM<sub>BC</sub> concentration and light absorption  
 157 coefficients (b<sub>abs</sub>) increased in the latter period of Xihai campaign, contrasting with the marked decreasing pattern in PM<sub>BC</sub>  
 158 concentration and b<sub>abs</sub> observed during the latter period of Lulang campaign. In Xihai, the concentration and proportion of  
 159 inorganic components, especially NO<sub>3</sub><sup>-</sup>, rose in the latter phase of the campaign as the wind direction (WD) shifted to south-  
 160 easterly (Fig. 2f). The RH also got higher with the change of wind direction. Another major feature is that the wind direction  
 161 had distinct diurnal variations. In Xihai, the wind direction converted from easterly and northeasterly flows during the nocturnal  
 162 hours to southerly direction during daytime. Conversely, Lulang is predominantly controlled by northerly to northeasterly  
 163 winds throughout the campaign period. Nevertheless, the wind speed (WS) were similar in Xihai and Lulang, with mean value  
 164 of 1.8 ± 1.2 m s<sup>-1</sup> and 1.5 ± 1.2 m s<sup>-1</sup>, respectively. In terms of gaseous pollutants, higher levels of NO<sub>x</sub> and O<sub>3</sub> were observed  
 165 in Xihai (5.3 ± 3.4 and 48 ± 13 ppb) than in Lulang (4.0 ± 2.5 and 35 ± 15 ppb).

167 **Table 1: Overview of the BC concentration (mean $\pm$ 1 $\sigma$ ) at different sites of TP in existing studies. The minimum value and maximum**  
 168 **value were shown in the parenthesis. The measurement result was divided by black lines in the table based on different measurement**  
 169 **techniques.**

Sampling Site	Location	Instrument	Sampling period (Year.Month)	Altitude(m)	BC concentration ( $\mu\text{g m}^{-3}$ )	Reference
Lulang	Southeastern TP	SP-AMS	2021.04-2021.05	3300	0.17 $\pm$ 0.17 (0.02-2.22)	This study
Xihai	Northeastern TP	SP-AMS	2021.06	3300	0.24 $\pm$ 0.20 (0.02-1.28)	This study
Qinghai Lake	Northeastern TP	SP2	2011.10	3200	0.36 $\pm$ 0.27 (0.05-1.56)	Wang et al., 2014
Nam Co	Central TP	SP-AMS	2015.05-2015.06	4730	0.12 $\pm$ 0.085	Wang et al., 2017
Linzhi	Southeastern TP	AE 16	2008.11-2009.01	3300	0.75 (0.30-1.60)	Cao et al., 2010
Lulang	Southeastern TP	AE 16	2008.07-2009.08	3300	0.50 $\pm$ 0.52 (0.06-5.37)	Zhao et al., 2017
Mt. Muztagh Ata	Western TP	AE 16	2009.11-2010.09	4500	0.13 $\pm$ 0.06 (0.03-0.33)	Zhu et al., 2016
Hanle valley	Southern TP	AE 31	2009.08-2010.07	4250	0.077 $\pm$ 0.064 (0.007-0.30)	Babu et al., 2011
Lulang	Southeastern TP	OC/EC Analyzer	2008.07-2009.07	3300	0.52 $\pm$ 0.04	Zhao et al., 2013
QOMS	Southern TP	OC/EC Analyzer	2009.08-2010.07	4276	0.25 $\pm$ 0.22	Cong et al., 2015
Manora Peak	Southern TP	OC/EC Analyzer	2005.02-2007.06	1950	1.0 $\pm$ 0.7 (0.1-2.7)	Ram and Sarin, 2009

170 We also compared the observed BC concentration at different sites of TP. Note that, the term “black carbon (BC)” has  
 171 not been used rigorously or consistently throughout all previous modelling and measurement literature (Bond et al., 2013).  
 172 Similar terms including “rBC”, “eBC”, and “EC” has also been widely used corresponding to different measurement  
 173 techniques. BC measured by laser-induced techniques is often referred as “rBC”, and measured BC using light absorption (e.g.  
 174 Aethalometer, AE) and thermal/optical methods are normally named as “the equivalent BC (eBC)” and “elemental carbon  
 175 (EC)”, respectively. In Table 1, BC concentrations in TP measured by several common techniques were collected and grouped  
 176 according to the methods to make clearer comparison. Compared to measurements using the same instrument in a metropolitan  
 177 area (Cui et al., 2022), the rBC concentration of TP (0.24 $\pm$ 0.20  $\mu\text{g m}^{-3}$ ) was approximately 25% or less of Shanghai (0.92 $\pm$   
 178 0.81  $\mu\text{g m}^{-3}$ ). The rBC concentration in Xihai was relatively high compared to southeastern and central TP measured using  
 179 same technique (Table 1). This was potentially attributed to the strong BC emissions in surrounding area of northeast TP (Fig.  
 180 1). The rBC concentration in Lulang exhibited a relatively lower mean value yet with a broad range of variation, suggesting  
 181 that BC may be subject to diverse airmasses with significant discrepancies in emission intensity across the southeast and  
 182 southern regions of the TP (Fig. 1). Higher BC levels were observed at stations in proximity to the Indo-China Peninsula and  
 183 South Asia where wildfire activities were extremely intense in spring. Therefore, the considerable variability of rBC  
 184 concentrations in Lulang is likely due to the alternating influences from airmasses transporting BB plume and those originating  
 185 from cleaner environments.

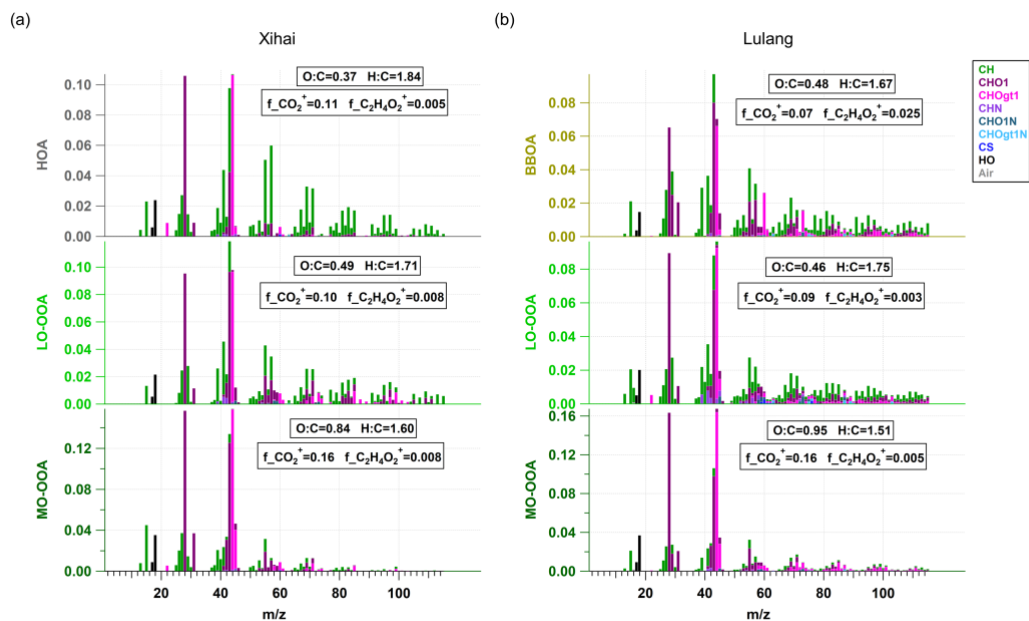




187

188 **Figure 3: The box plots of (a) rBC and (b) BC-containing particles mass concentrations in Xihai and Lulang, the lower and upper**  
 189 **lines of box plot represent the 25<sup>th</sup> and 75<sup>th</sup> percentiles and the whiskers stand for 5<sup>th</sup> and 95<sup>th</sup> values. The charts of normalized**  
 190 **frequency distribution show (c) mass ratio of coating substance to rBC core ( $R_{\text{BC}}$ ) and (d) mass absorption cross-section (MAC).**  
 191 **Only 1.15% of the  $R_{\text{BC}}$  exceeded the maximum value of bin (19.5) in Xihai, and no  $R_{\text{BC}}$  exceeded the maximum value of bin in Lulang.**

192 The overall characteristic of  $\text{PM}_{\text{BC}}$  in Xihai and Lulang was compared based on statistical results. As Fig. 3a and Fig. 3b  
 193 show, the mass concentration of rBC and  $\text{PM}_{\text{BC}}$  were higher in Xihai due to possible impacts of stronger anthropogenic  
 194 emissions (Fig. 1b), and the difference ( $t_{\text{rBC}}=2.8$ ,  $t_{\text{PMBC}}=2.1$ ) between the two sites was proved by the t-test ( $\alpha=0.05$ ,  $v=50$ ).  
 195 Figure 3c compares mixing state of  $\text{PM}_{\text{BC}}$  in Xihai and Lulang, which was expressed by the mass ratio of BC coating to rBC  
 196 ( $R_{\text{BC}}$ ). The frequency distribution of  $R_{\text{BC}}$  had obvious difference at two sites.  $R_{\text{BC}}$  in Xihai was generally higher than in Lulang,  
 197 indicating the thicker coating in Xihai. The peak of  $R_{\text{BC}}$  occurred at [4.5,6] and [1.5,3] in Xihai and Lulang, respectively.  $R_{\text{BC}}$   
 198 of more than 50%  $\text{PM}_{\text{BC}}$  was between 3.0 and 7.5, and only 11%  $\text{PM}_{\text{BC}}$  had  $R_{\text{BC}}$  less than 3.0 in Xihai. Unlike Xihai, the  
 199 percentage of thinly coated  $\text{PM}_{\text{BC}}$  that  $R_{\text{BC}}$  was less than 3.0 was higher to 33% in Lulang. The difference on mixing states of  
 200  $\text{PM}_{\text{BC}}$  was also demonstrated by the t-test ( $t_{R_{\text{BC}}}=2.4$ ). The peak of MAC at both sites was between 12 and 14  $\text{m}^2 \text{g}^{-1}$  (Fig. 3d)  
 201 which was significantly greater than the MAC of BC without coating (Bond and Bergstrom, 2006), and average value and  
 202 range of MAC in Xihai and Lulang was 12.8 (5.6-17.4) and 12.3 (6.8-15.7)  $\text{m}^2 \text{g}^{-1}$ . Over 61% of BC was distributed in larger  
 203 MAC range (higher than 12.5  $\text{m}^2 \text{g}^{-1}$ ) in Xihai, showing stronger light absorption ability of BC in this region. Due to the  
 204 synergy of higher mass concentration and light absorption ability,  $\text{PM}_{\text{BC}}$  could bring larger climate effects in northeast TP.

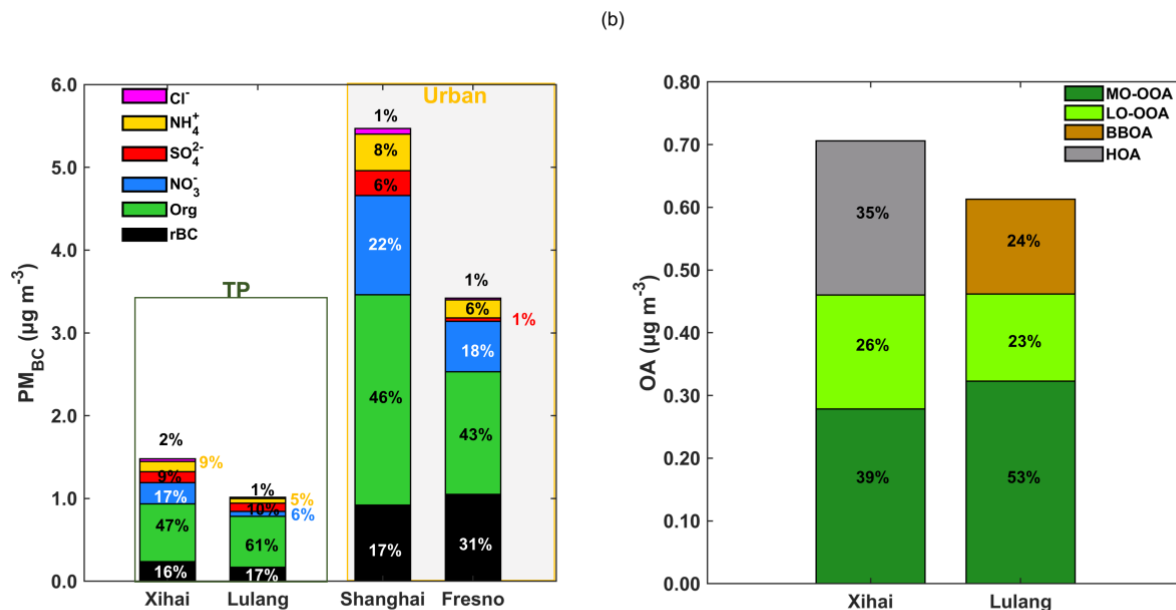


205

206 **Figure 4: The mass spectra of different factors represents the organic aerosol from specific sources in BC-containing particles in (a)**  
 207 **Xihai and (b) Lulang. MO-OOA is more oxidized oxygenated organic aerosol, LO-OOA is less oxidized oxygenated organic aerosol,**  
 208 **HOA is hydrocarbon-like organic aerosol and BBOA is biomass burning organic aerosol.**

209 The chemical characteristics and sources of OA in  $PM_{BC}$  were identified by PMF. OA was separated into primary OA  
 210 (POA) and oxygenated OA (OOA) at both sites (Fig.4 and Fig. S2). In Xihai, there were one factor originating from primary  
 211 emissions and two factors from secondary formation. The POA factor had higher signal of  $C_4H_7^+$  and  $C_4H_9^+$ , which is the  
 212 important alkyl fragments from primary sources (Hu et al., 2016), in its mass spectrum. It also had higher content of hydrogen  
 213 that H:C was up to 1.84 and lower signal of  $C_2H_3O^+$  which is the typical BB tracer. Hence, this factor was mainly emitted from  
 214 fossil fuel combustion rather than BB, and was named as Hydrocarbon OA (HOA). OOA factors were further divided into  
 215 less-oxidized OOA (LO-OOA) and more-oxidized OOA (MO-OOA) factors. These two factors were secondary OA (SOA)  
 216 formed through oxidation processes such as photochemical reactions (Kanakidou et al., 2005; Zhang et al., 2005a; Zhao et al.,  
 217 2018). They had higher fraction of signal of  $CO_2^+$  ion (m/z 44) and other oxygenic ions in mass spectrum, which is similar to  
 218 the mass spectra of typical OOA reported in other field campaigns (Crippa et al., 2013; Hu et al., 2016; Kim et al., 2020; Lee  
 219 et al., 2017; Sun et al., 2020; Wang et al., 2016; Zhou et al., 2018). The O:C of the two OOA factors was also calculated  
 220 (Canagaratna et al., 2015) to learn about the oxidation degree of OOA. MO-OOA exhibited higher O:C ratio (0.84) than LO-  
 221 OOA (0.49). Unlike Xihai, the POA factor in Lulang had higher fraction of signal of  $C_2H_3O^+$  (m/z 60) ion ( $f_{C_2H_3O^+}$ ) in mass  
 222 spectrum, which is the fragment of levoglucosan mainly from BB (Lee et al., 2010). Therefore, this POA factor was identified  
 223 as biomass burning OA (BBOA) in Lulang. Moreover, the  $f_{CO_2^+}$  and  $f_{C_2H_4O_2^+}$  (0.065 versus 0.025) of this factor were also  
 224 within the triangle area in previous BBOA study (Cubison et al., 2011), and the  $f_{C_2H_4O_2^+}$  was lower than the fresh BBOA,  
 225 indicating that this factor was influenced by biomass burning activities and aging processes collectively. The remaining two

226 factors were from SOA formation in Lulang, and had higher fraction of signal of  $\text{CO}_2^+$  ion. Based on the oxidation degree, the  
 227 two factors were identified as MO-OOA and LO-OOA. The O:C of MO-OOA and LO-OOA was 0.95 and 0.46, respectively.  
 228 Compared to Lulang, the OA in BC coating was under stronger impacts of anthropogenic emissions in Xihai indicated by  
 229 HOA.

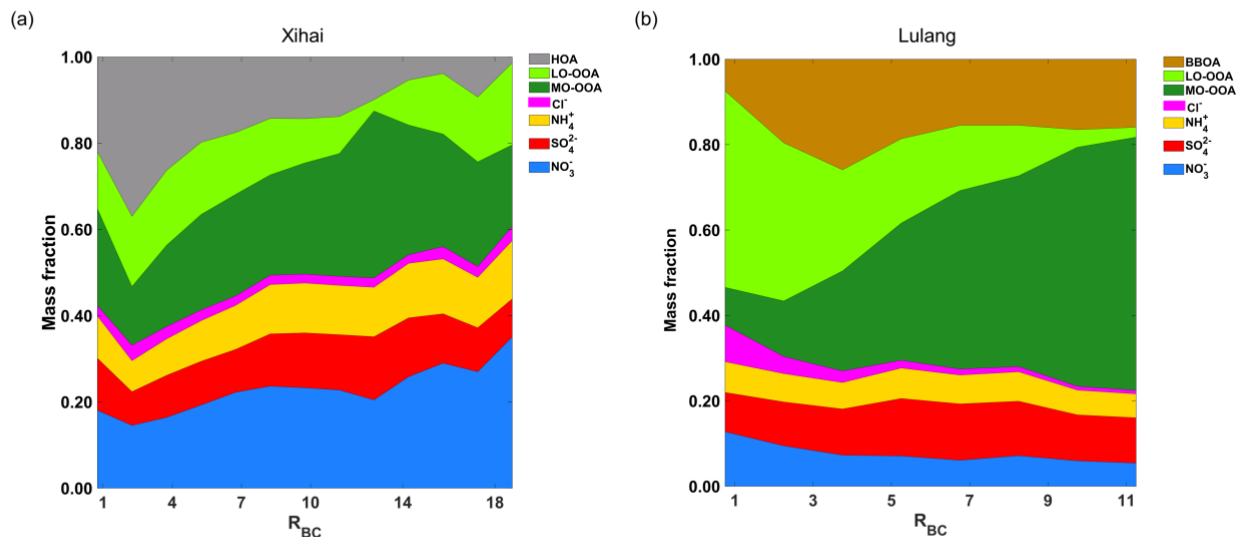


230

231 **Figure 5: The stacked bars represent mass concentrations of (a) different species in BC-containing particles ( $\text{PM}_{\text{BC}}$ ), and (b) different**  
 232 **factors of organic aerosol in BC-containing particles. The numbers on the plot show the percentage of different species and organic**  
 233 **factors. In subplot (a),  $\text{PM}_{\text{BC}}$  in the TP (this study) was compared to  $\text{PM}_{\text{BC}}$  in urban regions (Collier et al., 2018; Cui et al., 2022).**

234 Figure 5 presents  $\text{PM}_{\text{BC}}$  chemical composition at two sites. BC coating had higher mass contribution to  $\text{PM}_{\text{BC}}$  in Xihai  
 235 and Lulang compared to the urban site (Collier et al., 2018), indicating the thick coating of  $\text{PM}_{\text{BC}}$  in TP. The average mass  
 236 fraction and concentration of BC coating were 84% and  $1.2 \mu\text{g m}^{-3}$  in Xihai. The mass fraction of coating was similar (83%)  
 237 in Lulang, although the concentration of BC coating was lower ( $0.85 \mu\text{g m}^{-3}$ ). OA was the dominant component of BC coating  
 238 (Fig. 5a) at both sites, which was consistent with the observation in central TP (Wang et al., 2017). OA took up a higher  
 239 proportion in BC coating in Lulang compared to Xihai, Shanghai (Cui et al., 2022) and Fresno (Collier et al., 2018). During  
 240 the field campaign, the average concentration of HOA, LO-OOA and MO-OOA was  $0.25$ ,  $0.18$  and  $0.28 \mu\text{g m}^{-3}$  in Xihai. MO-  
 241 OOA also had the highest concentration ( $0.32 \mu\text{g m}^{-3}$ ) of OA in Lulang, and exceeded BBOA ( $0.15 \mu\text{g m}^{-3}$ ) and LO-OOA  
 242 concentration ( $0.14 \mu\text{g m}^{-3}$ ). It demonstrated that SOA formation plays an important role in coating process of  $\text{PM}_{\text{BC}}$ . The BC  
 243 coating was dominated by MO-OOA which was importantly affected by atmospheric oxidizing process. The concentration of  
 244  $\text{O}_3$  highly relative to atmospheric oxidizing capacity improved significantly in afternoon (Fig. S8), and the enhanced oxidizing

245 capacity could cause increase of MO-OOA in BC coating in both Xihai and Lulang. Besides MO-OOA,  $\text{NO}_3^-$  (17%) and HOA  
 246 (35%) also made large contribution on BC coating (Fig. 5a) and coated OA (Fig. 5b) in Xihai compared to Lulang. The HOA  
 247 and  $\text{NO}_3^-$  were both closely associated with anthropogenic sources because the anthropogenic sources emitted the HOA (Zhang  
 248 et al., 2005a) and precursors of  $\text{NO}_3^-$  largely (Dall'osto et al., 2009; Richter et al., 2005; Sun et al., 2018). It indicated that  
 249 anthropogenic emissions have a strong influence on coating process of  $\text{PM}_{\text{BC}}$  in northeast TP, which is quite different from  
 250 southeast TP.



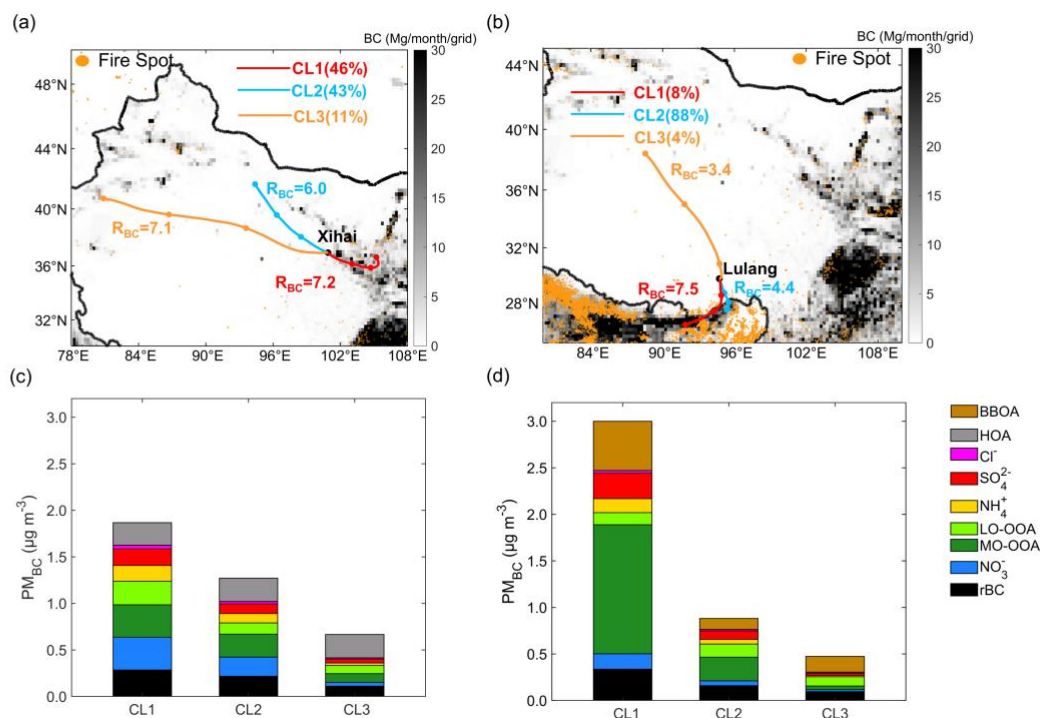
251

252 **Figure 6: The variation of BC coating composition with  $R_{\text{BC}}$  between (a) Xihai and (b) Lulang. The x-axis represents the mass ratio**  
 253 **of BC coating components and rBC cores ( $R_{\text{BC}}$ ), and the y-axis represents the mass fractions of BC coating components coated on**  
 254 **rBC. The mass fraction of components was averaged in each bin of  $R_{\text{BC}}$  (bin width: 1.5).**

255 Figure 6 shows the coating components of BC with different  $R_{\text{BC}}$  in Xihai and Lulang. The mass fraction of MO-OOA  
 256 was predominant in the thick-coated  $\text{PM}_{\text{BC}}$  in both Xihai and Lulang. Notably, a more significant enhancement in MO-OOA  
 257 contribution within the thickly coated  $\text{PM}_{\text{BC}}$  was exhibited in Lulang, concomitant with a reduced fraction of inorganic  
 258 components. The mass fraction of MO-OOA was only 9% in the thin BC coating ( $R_{\text{BC}} < 1.5$ ), rising dramatically to 59% in  
 259 those with  $R_{\text{BC}}$  exceeding 10.5 (thick BC coating). Another notable feature of the coating components was the higher  
 260 contribution of BBOA in Lulang, especially when the coating thickness of  $\text{PM}_{\text{BC}}$  was higher. It indicated that thickly coating  
 261 of BC was affected by BB activities and atmospheric oxidation significantly. In contrast to Lulang, HOA contribution  
 262 decreased with the growth of  $R_{\text{BC}}$ , indicating a weaker effect of primary aerosol on thickly-coated  $\text{PM}_{\text{BC}}$  in Xihai. Besides the  
 263 MO-OOA,  $\text{NO}_3^-$  also contributed significantly to the composition of thickly-coated  $\text{PM}_{\text{BC}}$  in Xihai, while the contribution of

264  $\text{NO}_3^-$  dropped with the rise of  $R_{\text{BC}}$  in Lulang. As illustrated in Fig. 6a, the mass fraction of  $\text{NO}_3^-$  reached to 35% in the maximum  
 265 bin of  $R_{\text{BC}}$  (18-19.5) in Xihai. The abundant  $\text{NO}_3^-$  was closely associated with anthropogenic sources as mentioned in the  
 266 preceding paragraph. The results demonstrate substantial variability in the composition influencing BC aging across TP  
 267 affected by diverse emission sources. Moreover, anthropogenic pollutant emissions had strong impacts on BC coating even in  
 268 the remote highland areas, and the contribution of inorganic aerosol to BC coating is non-negligible in TP.

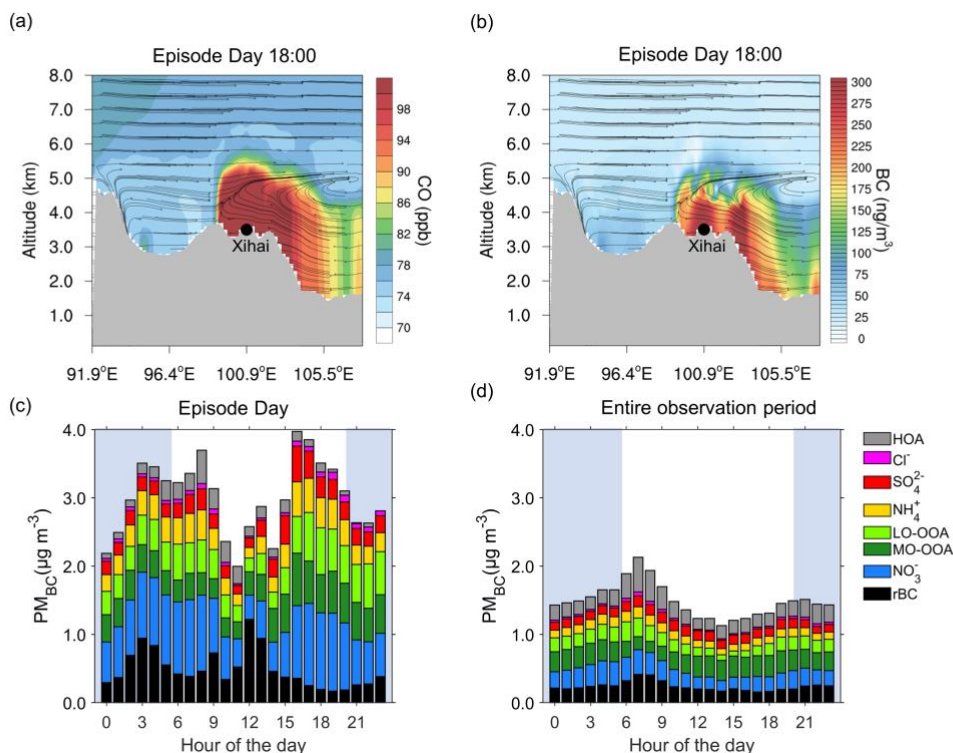
### 269 3.3 Impacts of transported emissions on BC-containing particles



270  
 271 **Figure 7: The maps show the backward trajectories in different clusters of (a) Xihai and (b) Lulang. Each circular marker along the**  
 272 **trajectories denotes a 24-hour interval. The background shading represents the anthropogenic BC emission intensity and the orange**  
 273 **spots represent the location of wildfire during the campaign in (a) and (b). The stacked bar plots show the mass concentration of**  
 274 **coating components and rBC in (c) Xihai and (d) Lulang.**

275 As discussed above,  $\text{PM}_{\text{BC}}$  in TP region is possibly affected by both anthropogenic sources and BB transported from  
 276 surrounding areas. To further investigate the impact mechanism of regional transport on BC, the cluster analysis of backward  
 277 trajectories was carried out during field campaign of Xihai and Lulang, and backward trajectories were clustered into three  
 278 kinds. In Xihai, the airmasses were dominantly from eastern region outside of TP, as indicated by airmasses cluster1 (CL1),  
 279 followed by the airmasses of cluster2 (CL2) from the northwest of Xihai, and the airmasses of cluster3 (CL3) from west of  
 280 Xihai (Fig. 7a).  $\text{PM}_{\text{BC}}$  was brought more to Xihai (Fig. 7c) by the airmasses of CL1 which went through the lower-altitude  
 281 regions with stronger anthropogenic BC emissions (Fig. 7a and Fig. 1b). In Lulang, the CL1 airmasses from South Asia were

282 heavily polluted and aged, the CL2 airmasses from southern edge of Himalayas and the CL3 airmasses from central inland of  
283 TP were cleaner (Fig. 7b). Comparing the polluted airmasses (CL1) at two sites, chemical composition of  $\text{PM}_{\text{BC}}$  showed  
284 obvious difference between Xihai and Lulang (Fig. 7c and 7d). The contribution of inorganic species to BC coating was higher  
285 in Xihai, and there was more OA (especially MO-OOA) in polluted airmass of Lulang. MO-OOA was the major component  
286 of BC coating in CL1 in Lulang. As shown by Fig. 7b, there was intensive wildfire in the source region of CL1 airmasses of  
287 Lulang, and the wildfire plume could be readily uplifted to higher altitude due to prevailing upflow driven by the lifting of the  
288 plume (Freitas et al., 2007; Fromm et al., 2000; Labonne et al., 2007; Luderer et al., 2006; Sofiev et al., 2012) or large-scale  
289 westerly and small-scale southerly circulations during the pre-monsoon season (Zhang et al., 2020; Cao et al., 2010). Such  
290 circulation could transport BC and other co-emitted pollutants from wildfires in Indo-China Peninsula and South Asia over the  
291 mountain of TP and reached Lulang. Because the biomass burning during wildfires can emit plentiful volatile organic  
292 compounds (VOCs) like terpenes (Akagi et al., 2013; Fiddler et al., 2024), it is expected that SOA can be formed through  
293 oxidation from precursors in the plume, leading to a thick coating on  $\text{PM}_{\text{BC}}$ . In Xihai,  $\text{NO}_3^-$  was one of the major coating  
294 species in  $\text{PM}_{\text{BC}}$  in CL1 (Fig. 7c) with mass concentration of  $\text{NO}_3^-$  up to  $0.35 \mu\text{g m}^{-3}$  (accounts for 19% of  $\text{PM}_{\text{BC}}$ ), and other  
295 airmasses clusters had higher mass fraction of HOA in BC coating indicating that  $\text{PM}_{\text{BC}}$  was less affected by oxidation and  
296 was fresher. CL1 transported from northwest region of China where the anthropogenic emissions are much stronger than TP  
297 (Fig. 7a). With higher concentrations of primary pollutants like  $\text{NO}_x$ , the formation and coating of  $\text{NO}_3^-$  can be enhanced in  
298  $\text{PM}_{\text{BC}}$ . Above results indicated that the effects of emission sources were discrepant in different regions of TP, and the northeast  
299 part of the TP was significantly affected by anthropogenic emissions.



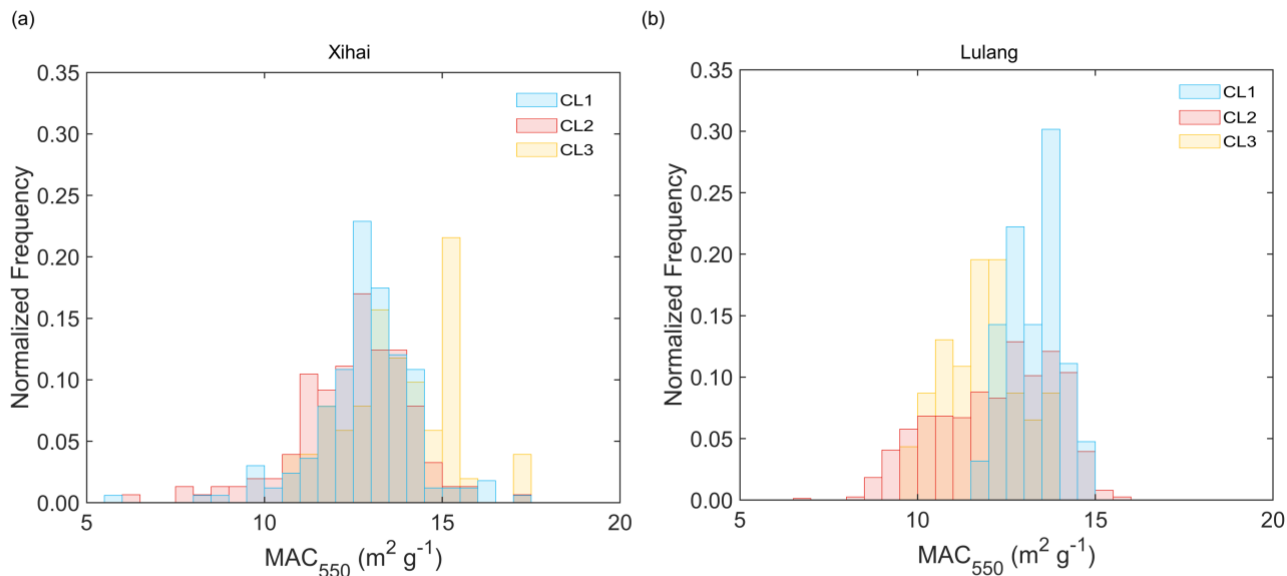
300

301 **Figure 8: Simulated meridional mean concentration profile of (a) CO and (b) BC independently during the episode day (19 June,**  
 302 **2021). The air circulation is shown as vector arrows and the terrain height is shown as gray shade in (a) and (b) subplots. The vertical**  
 303 **velocity of wind was amplified by a factor of 3000 for clarity. The (c) and (d) subplots show the diurnal variation of BC-containing**  
 304 **particles concentration during the (c) episode day and (d) entire observation period in Xihai. The blue shade represents the nighttime**  
 305 **hours during Xihai campaign in (c) and (d) subplots. The sunrise on Xihai was about 6:00 a.m. (Beijing Time), and sunset was about**  
 306 **8:30 p.m. (Beijing Time).**

307 To further explore the coupling effect of horizontal and vertical transport on BC in high-altitude region, both observation  
 308 and simulation were performed to track the evolution of pollutants in surrounding area. We chose a typical episode in CL1 in  
 309 Xihai to conduct model simulation. As illustrated in the meridional profile plots of CO and BC, the high levels of anthropogenic  
 310 pollutants were uplifted to Xihai (Fig. 8a and Fig. 8b). The updraft flow and the turbulent mixing in the boundary layer carried  
 311 the anthropogenic emissions from the ground to the high altitude, and then the horizontal easterly winds transported the  
 312 anthropogenic emissions to the northeast TP. The combination of upward wind and developing boundary layer (Fig. S8c)  
 313 allowed the pollutants emitted by the anthropogenic sources near the surface to be carried aloft and transported to high-altitude  
 314 TP in the afternoon. This effect can significantly change both the concentration and chemical composition of BC. Compared  
 315 to the average diurnal variation during observation period, the diurnal variation during episode shows distinctive features (Fig.  
 316 8c and 8d). PM<sub>BC</sub> concentration increased remarkably from 15:00 and peaked at 16:00 to 17:00 with a maximum concentration  
 317 of 4.0 μg m<sup>-3</sup>. Concurrently, NO<sub>3</sub><sup>-</sup> and SOA also exhibit a noticeable increase along with the thickening BC coating in the  
 318 afternoon. The NO<sub>3</sub><sup>-</sup>, SOA, and R<sub>BC</sub> rose from 0.41 μg m<sup>-3</sup>, 0.49 μg m<sup>-3</sup>, and 2.8 at 11:00 to 1.06 μg m<sup>-3</sup>, 1.31 μg m<sup>-3</sup>, and  
 319 10.2 at 16:00, respectively. As the Fig. S8a shows, O<sub>3</sub> did not increased significantly after 3:00 p.m. in Xihai, implying that

320 the photochemistry and secondary aerosol formation might not enhance. However, the consistent radiative heating of the  
 321 ground surface during the daytime kept a convective boundary layer (Fig. S8c), facilitating the vertical transport of  
 322 anthropogenic emissions to higher altitudes and plausibly causing the enhanced air pollution in the afternoon in Xihai. This  
 323 phenomenon is a good illustration of the vulnerability of remote plateau regions to intense anthropogenic influences, as  
 324 pollutants can be transported from low-altitude regions to the plateau.

### 325 3. 4 Impacts of diverse BC coating characteristics on light absorption



326  
 327 **Figure 9: The normalized frequency distribution of MAC at 550 nm wavelength in different trajectory clusters of (a) Xihai and (b)**  
 328 **Lulang.**

329 The effects of different emission sources on the BC light absorption ability were investigated. Compared to Lulang, the  
 330 MAC of PM<sub>BC</sub> was overall higher in Xihai, indicating higher absorption efficiency and potentially stronger radiative forcing  
 331 in this region. The MAC were all relatively high in three clusters of airmasses of Xihai, with distribution peaked between 12  
 332 and 14 m<sup>2</sup> g<sup>-1</sup> that numerically comparable to previous studies (Wang et al., 2015). The overall high MAC in Xihai may result  
 333 from the significant impact of anthropogenic emissions in northeast TP. The stronger emissions provided abundant precursor  
 334 of BC coating to improve the coating thickness, and the thick coating enhance light absorption capacity of PM<sub>BC</sub> via “lensing  
 335 effect”. While MAC was higher only under control of the polluted CL1 airmasses in Lulang, indicating that the South Asian  
 336 wildfire plume could significantly strengthen the light absorption ability of BC. The MAC in Lulang was also comparable to



337 previous studies (Wang et al., 2018) that the peak of MAC distribution was  $7.6 \text{ m}^2 \text{ g}^{-1}$  at 870 nm ( $12.0 \text{ m}^2 \text{ g}^{-1}$  at 550 nm if the  
338 Absorption Ångström Exponent of BC is 1.0). In CL1 airmasses of Lulang, MAC mainly distributed at the bin between 12 and  
339  $14 \text{ m}^2 \text{ g}^{-1}$  that is close to MAC ( $13.1 \text{ m}^2 \text{ g}^{-1}$  at 550 nm) at other TP sites affected by biomass burning plume (Tan et al., 2021).  
340 The BC coating was thick (Fig. 7d) to improve the MAC in CL1 airmasses of Lulang influenced by higher BB emissions.  
341 These results indicate that strong BB and anthropogenic emissions from surrounding area could make noticeable impacts on  
342 chemical composition and light absorption ability of BC in TP, and these impacts were more prevalent in the northeast part of  
343 the TP.

#### 344 **4 Conclusions**

345 In this study, we employed the SP-AMS with a laser vaporizer only to quantitatively analyze the chemical composition  
346 of  $\text{PM}_{\text{BC}}$  at distinct sites, Xihai and Lulang, located in the northeast and southeast regions of the TP. Our findings demonstrate  
347 the considerable variability and spatial heterogeneity of BC physical and chemical properties across the TP. Notably, Xihai  
348 exhibited higher mass concentrations of rBC and  $\text{PM}_{\text{BC}}$ , with respective mean concentrations of  $0.24 \mu\text{g m}^{-3}$  and  $1.48 \mu\text{g m}^{-3}$ ,  
349 compared to  $0.17 \mu\text{g m}^{-3}$  and  $1.02 \mu\text{g m}^{-3}$  in Lulang. The  $\text{PM}_{\text{BC}}$  in Xihai has higher aging degree, as indicated by a higher mean  
350  $R_{\text{BC}}$  of 6.7, contrasting the mean  $R_{\text{BC}}$  of 4.5 in Lulang.

351 The marked differences in chemical composition of  $\text{PM}_{\text{BC}}$  were also observed within TP region. Due to differences in  
352 emission sources, the POA was distinct in Xihai and Lulang. HOA from fossil fuel combustion was one of the main  
353 components of  $\text{PM}_{\text{BC}}$  in Xihai as the result of elevated anthropogenic emissions, and there was more BBOA in Lulang  
354 especially when the airmasses were from South Asia Plain affected by frequent wildfire. Besides primary species, the  
355 secondary coating components also showed larger differences. The contribution of secondary inorganic aerosols, particularly  
356  $\text{NO}_3^-$  was noticeably higher in Xihai because of the strong anthropogenic emission of  $\text{NO}_x$  as the precursor of  $\text{NO}_3^-$ . SOA was  
357 comparatively higher in areas with less anthropogenic emissions like Lulang. The oxidizing level of SOA was high in both  
358 sites of TP that the MO-OOA occupied the largest mass fraction of SOA. We also investigated the variation of  $\text{PM}_{\text{BC}}$   
359 composition with its coating thickness in both sites. A marked enhancement in  $\text{NO}_3^-$  fraction was observed on aged BC coating  
360 in Xihai. In contrast, the mass contribution of  $\text{NO}_3^-$  decreased and SOA contribution notably increased during the thickening  
361 of  $\text{PM}_{\text{BC}}$  in Lulang.

362 Backward trajectory analysis and regional chemical transport modeling were then performed to track the impacts of  
363 transported anthropogenic and BB emissions on chemical composition of  $\text{PM}_{\text{BC}}$  in northeastern and southeastern TP. The effect  
364 of anthropogenic emissions was stronger in northeastern TP when the airmasses were brought by updrafts and easterly winds  
365 from lower-altitude areas, leading to an increase of  $\text{NO}_3^-$  and SOA coated on BC. With the development of boundary layer,  
366 strong turbulent mixing promoted the elevation of anthropogenic pollutants. In contrast to Xihai, the thickly coated BC in  
367 Lulang was mainly caused by elevation and transportation of biomass burning plume from the South Asia, leading to a  
368 significantly increased contribution of MO-OOA and BBOA. The distinct transported emissions caused substantial variations

369 of chemical composition and mixing state of BC, which further changes the light absorption ability of BC in the TP. The MAC  
370 of  $PM_{BC}$  at both sites was at a high level, showing the strong absorption ability of BC in TP region, especially in polluted  
371 airmasses affected by biomass burning emission from the South Asia. The overall thicker coating and higher MAC of  $PM_{BC}$   
372 in airmasses elevated from lower-altitude regions reveals the impacts of promoted BC aging processes during transportation  
373 on the mixing state and light absorption of BC in TP, which will further influence its radiative effects. Such impact needs to  
374 be considered in the evaluation of BC radiative effects for the TP region.

#### 375 **Data availability**

376 The wildfire emission data FINN is available at <https://www.acom.ucar.edu/Data/fire/>. The anthropogenic emission data MIX  
377 is available at <http://www.meicmodel.org/dataset-mix.html>. The BLH is acquired from the fifth-generation European Centre  
378 for Medium-Range Weather Forecasts (ECMWF) reanalysis data (ERA5; <https://cds.climate.copernicus.eu/cdsapp#!/home>).  
379 The measurement data covered in the article can be found at: <https://doi.org/10.6084/m9.figshare.25399024>. Additional data  
380 related to this paper may be requested from the authors.

#### 381 **Author contribution**

382 CF, AD, and JPW conceptualized and supervised this study. JBW, YZ, TL, XC, DG, CZ, LW, XQ and WN conducted the  
383 field campaign. JBW and JPW conducted the data analysis. SL and XH contributed to the model development and simulation.  
384 JBW wrote the draft and drew the plots. JPW, XH and QZ discussed the results. JBW and JPW reviewed and edited the paper  
385 with contributions from all co-authors.

#### 386 **Competing interests**

387 The contact author has declared that none of the authors has any competing interests.

#### 388 **Acknowledgments**

389 This work was supported by the second Tibetan Plateau Scientific Expedition and Research (STEP) program (2019QZKK0106)  
390 and the National Natural Science Foundation of China (42005082).

#### 391 **References**

392 Akagi, S. K., Yokelson, R. J., Burling, I. R., Meinardi, S., Simpson, I., Blake, D. R., McMeeking, G. R., Sullivan, A., Lee, T.,  
393 Kreidenweis, S., Urbanski, S., Reardon, J., Griffith, D. W. T., Johnson, T. J., and Weise, D. R.: Measurements of reactive

394 trace gases and variable O<sub>3</sub> formation rates in some South Carolina biomass burning plumes, *Atmospheric Chemistry and*  
395 *Physics*, 13, 1141-1165, 10.5194/acp-13-1141-2013, 2013.

396 Babu, S. S., Chaubey, J. P., Moorthy, K. K., Gogoi, M. M., Kompalli, S. K., Sreekanth, V., Bagare, S. P., Bhatt, B. C., Gaur,  
397 V. K., Prabhu, T. P., and Singh, N. S.: High altitude (~4520 m amsl) measurements of black carbon aerosols over  
398 western trans-Himalayas: Seasonal heterogeneity and source apportionment, *J Geophys Res-Atmos*, 116,  
399 10.1029/2011jd016722, 2011.

400 Bohren, C. F., and Huffman, D. R.: Absorption and scattering of light by small particles, Wiley Science Paperback Series,  
401 John Wiley & Sons, New York, NY, USA, 7, 7.5, 1983.

402 Bond, T. C. and Bergstrom, R. W.: Light absorption by carbonaceous particles: An investigative review, *Aerosol Science*  
403 *and Technology*, 40, 27-67, 10.1080/02786820500421521, 2006.

404 Bond, T. C., Doherty, S. J., Fahey, D. W., Forster, P. M., Berntsen, T., DeAngelo, B. J., Flanner, M. G., Ghan, S., Karcher,  
405 B., Koch, D., Kinne, S., Kondo, Y., Quinn, P. K., Sarofim, M. C., Schultz, M. G., Schulz, M., Venkataraman, C.,  
406 Zhang, H., Zhang, S., Bellouin, N., Guttikunda, S. K., Hopke, P. K., Jacobson, M. Z., Kaiser, J. W., Klimont, Z.,  
407 Lohmann, U., Schwarz, J. P., Shindell, D., Storelvmo, T., Warren, S. G., and Zender, C. S.: Bounding the role of black  
408 carbon in the climate system: A scientific assessment, *J Geophys Res-Atmos*, 118, 5380-5552, 10.1002/jgrd.50171,  
409 2013.

410 Cai, J., Wu, C., Wang, J. D., Du, W., Zheng, F. X., Hakala, S. M., Fan, X. L., Chu, B. W., Yao, L., Feng, Z. M., Liu, Y. C.,  
411 Sun, Y. L., Zheng, J., Yan, C., Bianchi, F., Kulmala, M., Mohr, C., and Daellenbach, K. R.: Influence of organic aerosol  
412 molecular composition on particle absorptive properties in autumn Beijing, *Atmospheric Chemistry and Physics*, 22,  
413 1251-1269, 10.5194/acp-22-1251-2022, 2022.

414 Canagaratna, M. R., Jimenez, J. L., Kroll, J. H., Chen, Q., Kessler, S. H., Massoli, P., Hildebrandt Ruiz, L., Fortner, E.,  
415 Williams, L. R., Wilson, K. R., Surratt, J. D., Donahue, N. M., Jayne, J. T., and Worsnop, D. R.: Elemental ratio  
416 measurements of organic compounds using aerosol mass spectrometry: characterization, improved calibration, and  
417 implications, *Atmospheric Chemistry and Physics*, 15, 253-272, 10.5194/acp-15-253-2015, 2015.

418 Canagaratna, M. R., Jayne, J. T., Jimenez, J. L., Allan, J. D., Alfarra, M. R., Zhang, Q., Onasch, T. B., Drewnick, F., Coe,  
419 H., Middlebrook, A., Delia, A., Williams, L. R., Trimborn, A. M., Northway, M. J., DeCarlo, P. F., Kolb, C. E.,  
420 Davidovits, P., and Worsnop, D. R.: Chemical and microphysical characterization of ambient aerosols with the  
421 aerodyne aerosol mass spectrometer, *Mass Spectrometry Reviews*, 26, 185-222, 10.1002/mas.20115, 2007.

422 Cao, J. J., Tie, X. X., Xu, B. Q., Zhao, Z. Z., Zhu, C. S., Li, G. H., and Liu, S. X.: Measuring and modeling black carbon  
423 (BC) contamination in the SE Tibetan Plateau, *Journal of Atmospheric Chemistry*, 67, 45-60, 10.1007/s10874-011-  
424 9202-5, 2010.

425 Chen, P. F., Kang, S. C., Li, C. L., Zhang, Q. G., Guo, J. M., Tripathee, L., Zhang, Y. A., Li, G., Gul, C., Cong, Z. Y., Wan,  
426 X., Niu, H. W., Panday, A. K., Rupakheti, M., and Ji, Z. M.: Carbonaceous aerosol characteristics on the Third Pole: A  
427 primary study based on the Atmospheric Pollution and Cryospheric Change (APCC) network, *Environmental Pollution*,  
428 253, 49-60, 10.1016/j.envpol.2019.06.112, 2019.

429 Chen, X. Y., Ye, C. X., Wang, Y. Y., Wu, Z. J., Zhu, T., Zhang, F., Ding, X. K., Shi, Z. B., Zheng, Z. H., and Li, W. J.:  
430 Quantifying evolution of soot mixing state from transboundary transport of biomass burning emissions, *Isience*, 26,  
431 10.1016/j.isci.2023.108125, 2023.

432 Cheng, Y., Engling, G., Moosmaller, H., Arnott, W. P., Chen, L. W. A., Wold, C. E., Hao, W. M., and He, K. B.: Light  
433 absorption by biomass burning source emissions, *Atmos Environ*, 127, 347-354, 10.1016/j.atmosenv.2015.12.045,  
434 2016.

435 Collier, S., Williams, L. R., Onasch, T. B., Cappa, C. D., Zhang, X. L., Russell, L. M., Chen, C. L., Sanchez, K. J., Worsnop,  
436 D. R., and Zhang, Q.: Influence of Emissions and Aqueous Processing on Particles Containing Black Carbon in a  
437 Polluted Urban Environment: Insights From a Soot Particle-Aerosol Mass Spectrometer, *J Geophys Res-Atmos*, 123,  
438 6648-6666, 10.1002/2017jd027851, 2018.

439 Cong, Z., Kang, S., Kawamura, K., Liu, B., Wan, X., Wang, Z., Gao, S., and Fu, P.: Carbonaceous aerosols on the south  
440 edge of the Tibetan Plateau: concentrations, seasonality and sources, *Atmospheric Chemistry and Physics*, 15, 1573-  
441 1584, 10.5194/acp-15-1573-2015, 2015.

442 Crippa, M., DeCarlo, P. F., Slowik, J. G., Mohr, C., Heringa, M. F., Chirico, R., Poulain, L., Freutel, F., Sciare, J., Cozic, J.,  
443 Di Marco, C. F., Elsasser, M., Nicolas, J. B., Marchand, N., Abidi, E., Wiedensohler, A., Drewnick, F., Schneider, J.,

444 Borrmann, S., Nemitz, E., Zimmermann, R., Jaffrezo, J. L., Prévôt, A. S. H., and Baltensperger, U.: Wintertime aerosol  
445 chemical composition and source apportionment of the organic fraction in the metropolitan area of Paris, *Atmospheric*  
446 *Chemistry and Physics*, 13, 961-981, 10.5194/acp-13-961-2013, 2013.

447 Cubison, M. J., Ortega, A. M., Hayes, P. L., Farmer, D. K., Day, D., Lechner, M. J., Brune, W. H., Apel, E., Diskin, G. S.,  
448 Fisher, J. A., Fuelberg, H. E., Hecobian, A., Knapp, D. J., Mikoviny, T., Riemer, D., Sachse, G. W., Sessions, W.,  
449 Weber, R. J., Weinheimer, A. J., Wisthaler, A., and Jimenez, J. L.: Effects of aging on organic aerosol from open  
450 biomass burning smoke in aircraft and laboratory studies, *Atmospheric Chemistry and Physics*, 11, 12049-12064,  
451 10.5194/acp-11-12049-2011, 2011.

452 Cui, S. J., Huang, D. D., Wu, Y. Z., Wang, J. F., Shen, F. Z., Xian, J. K., Zhang, Y. J., Wang, H. L., Huang, C., Liao, H., and  
453 Ge, X. L.: Chemical properties, sources and size-resolved hygroscopicity of submicron black-carbon-containing  
454 aerosols in urban Shanghai, *Atmospheric Chemistry and Physics*, 22, 8073-8096, 10.5194/acp-22-8073-2022, 2022.

455 Dall'Osto, M., Harrison, R. M., Coe, H., Williams, P. I., and Allan, J. D.: Real time chemical characterization of local and  
456 regional nitrate aerosols, *Atmospheric Chemistry and Physics*, 9, 3709-3720, 10.5194/acp-9-3709-2009, 2009.

457 DeCarlo, P. F., Kimmel, J. R., Trimborn, A., Northway, M. J., Jayne, J. T., Aiken, A. C., Gonin, M., Fuhrer, K., Horvath, T.,  
458 Docherty, K. S., Worsnop, D. R., and Jimenez, J. L.: Field-deployable, high-resolution, time-of-flight aerosol mass  
459 spectrometer, *Analytical Chemistry*, 78, 8281-8289, 10.1021/ac061249n, 2006.

460 Docherty, K. S., Jaoui, M., Corse, E., Jimenez, J. L., Offenberg, J. H., Lewandowski, M., and Kleindienst, T. E.: Collection  
461 Efficiency of the Aerosol Mass Spectrometer for Chamber-Generated Secondary Organic Aerosols, *Aerosol Science*  
462 *and Technology*, 47, 294-309, 10.1080/02786826.2012.752572, 2013.

463 Drewnick, F., Hings, S. S., DeCarlo, P., Jayne, J. T., Gonin, M., Fuhrer, K., Weimer, S., Jimenez, J. L., Demerjian, K. L.,  
464 Borrmann, S., and Worsnop, D. R.: A new time-of-flight aerosol mass spectrometer (TOF-AMS) - Instrument  
465 description and first field deployment, *Aerosol Science and Technology*, 39, 637-658, 10.1080/02786820500182040,  
466 2005.

467 Duan, A. M. and Wu, G. X.: Role of the Tibetan Plateau thermal forcing in the summer climate patterns over subtropical  
468 Asia, *Climate Dynamics*, 24, 793-807, 10.1007/s00382-004-0488-8, 2005.

469 Dusek, U., Reischl, G. P., and Hitzenberger, R.: CCN activation of pure and coated carbon black particles, *Environmental*  
470 *Science & Technology*, 40, 1223-1230, 10.1021/es0503478, 2006.

471 Fiddler, M. N., Thompson, C., Pokhrel, R. P., Majluf, F., Canagaratna, M., Fortner, E. C., Daube, C., Roscioli, J. R.,  
472 Yacovitch, T. I., Herndon, S. C., and Bililign, S.: Emission Factors From Wildfires in the Western US: An Investigation  
473 of Burning State, Ground Versus Air, and Diurnal Dependencies During the FIREX-AQ 2019 Campaign, *Journal of*  
474 *Geophysical Research-Atmospheres*, 129, 10.1029/2022jd038460, 2024.

475 Freitas, S. R., Longo, K. M., Chatfield, R., Latham, D., Dias, M., Andreae, M. O., Prins, E., Santos, J. C., Gielow, R., and  
476 Carvalho, J. A.: Including the sub-grid scale plume rise of vegetation fires in low resolution atmospheric transport  
477 models, *Atmospheric Chemistry and Physics*, 7, 3385-3398, 10.5194/acp-7-3385-2007, 2007.

478 Fromm, M., Alfred, J., Hoppel, K., Hornstein, J., Bevilacqua, R., Shettle, E., Servranckx, R., Li, Z. Q., and Stocks, B.:  
479 Observations of boreal forest fire smoke in the stratosphere by POAM III, SAGE II, and lidar in 1998, *Geophysical*  
480 *Research Letters*, 27, 1407-1410, 10.1029/1999gl011200, 2000.

481 Gao, M., Yang, Y., Liao, H., Zhu, B., Zhang, Y. X., Liu, Z. R., Lu, X., Wang, C., Zhou, Q. M., Wang, Y. S., Zhang, Q.,  
482 Carmichael, G. R., and Hu, J. L.: Reduced light absorption of black carbon (BC) and its influence on BC-boundary-  
483 layer interactions during "APEC Blue", *Atmospheric Chemistry and Physics*, 21, 11405-11421, 10.5194/acp-21-11405-  
484 2021, 2021.

485 Grell, G. A., Peckham, S. E., Schmitz, R., McKeen, S. A., Frost, G., Skamarock, W. C., et al. (2005), Fully coupled "online"  
486 chemistry within the WRF model, *Atmos. Environ.*, 39(37), 6957-6975. <https://doi.org/10.1016/j.atmosenv.2005.04.027>

487 Gustafsson, Ö. and Ramanathan, V.: Convergence on climate warming by black carbon aerosols, *P Natl Acad Sci USA*, 113,  
488 4243-4245, 10.1073/pnas.1603570113, 2016.

489 Henning, S., Wex, H., Hennig, T., Kiselev, A., Snider, J. R., Rose, D., Dusek, U., Frank, G. P., Pöschl, U., Kristensson, A.,  
490 Bilde, M., Tillmann, R., Kiendler-Scharr, A., Mentel, T. F., Walter, S., Schneider, J., Wennrich, C., and Stratmann, F.:  
491 Soluble mass, hygroscopic growth, and droplet activation of coated soot particles during LACIS Experiment in  
492 November (LEXNo), *J Geophys Res-Atmos*, 115, 10.1029/2009jd012626, 2010.

493 Hu, W. W., Hu, M., Hu, W., Jimenez, J. L., Yuan, B., Chen, W. T., Wang, M., Wu, Y. S., Chen, C., Wang, Z. B., Peng, J. F.,  
494 Zeng, L. M., and Shao, M.: Chemical composition, sources, and aging process of submicron aerosols in Beijing:  
495 Contrast between summer and winter, *J Geophys Res-Atmos*, 121, 1955-1977, 10.1002/2015jd024020, 2016.

496 Hua, S., Liu, Y. Z., Luo, R., Shao, T. B., and Zhu, Q. Z.: Inconsistent aerosol indirect effects on water clouds and ice clouds  
497 over the Tibetan Plateau, *International Journal of Climatology*, 40, 3832-3848, 10.1002/joc.6430, 2020.

498 Huang, X., Ding, A., Liu, L., Liu, Q., Ding, K., Niu, X., et al., 2016. Effects of aerosol-radiation interaction on precipitation  
499 during biomass-burning season in East China. *Atmos. Chem. Phys.* 16, 10063–10082.

500 Huang, X., Wang, Z., Ding, A., 2018. Impact of aerosol-PBL interaction on haze pollution: multiyear observational  
501 evidences in North China. *Geophys. Res. Lett.* 45, 8596–8603.

502 Huang, X., Ding, K., Liu, J. Y., Wang, Z. L., Tang, R., Xue, L., Wang, H. K., Zhang, Q., Tan, Z. M., Fu, C. B., Davis, S. J.,  
503 Andreae, M. O., and Ding, A. J.: Smoke-weather interaction affects extreme wildfires in diverse coastal regions,  
504 *Science*, 379, 457-461, 10.1126/science.add9843, 2023.

505 Kanakidou, M., Seinfeld, J. H., Pandis, S. N., Barnes, I., Dentener, F. J., Facchini, M. C., Van Dingenen, R., Ervens, B.,  
506 Nenes, A., Nielsen, C. J., Swietlicki, E., Putaud, J. P., Balkanski, Y., Fuzzi, S., Horth, J., Moortgat, G. K., Winterhalter,  
507 R., Myhre, C. E. L., Tsigaridis, K., Vignati, E., Stephanou, E. G., and Wilson, J.: Organic aerosol and global climate  
508 modelling: a review, *Atmospheric Chemistry and Physics*, 5, 1053-1123, 10.5194/acp-5-1053-2005, 2005.

509 Kang, S. C., Xu, Y. W., You, Q. L., Flügel, W. A., Pepin, N., and Yao, T. D.: Review of climate and cryospheric change in  
510 the Tibetan Plateau, *Environmental Research Letters*, 5, 10.1088/1748-9326/5/1/015101, 2010.

511 Kang, S. C., Zhang, Q. G., Qian, Y., Ji, Z. M., Li, C. L., Cong, Z. Y., Zhang, Y. L., Guo, J. M., Du, W. T., Huang, J., You,  
512 Q. L., Panday, A. K., Rupakheti, M., Chen, D. L., Gustafsson, Ö., Thiemens, M. H., and Qin, D. H.: Linking  
513 atmospheric pollution to cryospheric change in the Third Pole region: current progress and future prospects, *Natl Sci*  
514 *Rev*, 6, 796-809, 10.1093/nsr/nwz031, 2019.

515 Kim, H., Zhang, Q., and Sun, Y. L.: Measurement report: Characterization of severe spring haze episodes and influences of  
516 long-range transport in the Seoul metropolitan area in March 2019, *Atmospheric Chemistry and Physics*, 20, 11527-  
517 11550, 10.5194/acp-20-11527-2020, 2020.

518 Labonne, M., Bréon, F. M., and Chevallier, F.: Injection height of biomass burning aerosols as seen from a spaceborne lidar,  
519 *Geophysical Research Letters*, 34, 10.1029/2007gl029311, 2007.

520 Lack, D. A. and Cappa, C. D.: Impact of brown and clear carbon on light absorption enhancement, single scatter albedo and  
521 absorption wavelength dependence of black carbon, *Atmospheric Chemistry and Physics*, 10, 4207-4220, 10.5194/acp-  
522 10-4207-2010, 2010.

523 Lai, S., Qi, X., Huang, X., Lou, S., Chi, X., Chen, L., Liu, C., Liu, Y., Yan, C., Li, M., Liu, T., Nie, W., Kerminen, V. M.,  
524 Petäjä, T., Kulmala, M., and Ding, A.: New particle formation induced by anthropogenic–biogenic interactions on the  
525 southeastern Tibetan Plateau, *Atmos. Chem. Phys.*, 24, 2535-2553, 10.5194/acp-24-2535-2024, 2024.

526 Lee, A. K. Y., Chen, C. L., Liu, J., Price, D. J., Betha, R., Russell, L. M., Zhang, X. L., and Cappa, C. D.: Formation of  
527 secondary organic aerosol coating on black carbon particles near vehicular emissions, *Atmospheric Chemistry and*  
528 *Physics*, 17, 15055-15067, 10.5194/acp-17-15055-2017, 2017.

529 Lee, T., Sullivan, A. P., Mack, L., Jimenez, J. L., Kreidenweis, S. M., Onasch, T. B., Worsnop, D. R., Malm, W., Wold, C.  
530 E., Hao, W. M., and Collett, J. L.: Chemical Smoke Marker Emissions During Flaming and Smoldering Phases of  
531 Laboratory Open Burning of Wildland Fuels, *Aerosol Science and Technology*, 44, I-V,  
532 10.1080/02786826.2010.499884, 2010.

533 Li, M., Zhang, Q., Kurokawa, J., Woo, J. H., He, K. B., Lu, Z. F., Ohara, T., Song, Y., Streets, D. G., Carmichael, G. R.,  
534 Cheng, Y. F., Hong, C. P., Huo, H., Jiang, X. J., Kang, S. C., Liu, F., Su, H., and Zheng, B.: MIX: a mosaic Asian  
535 anthropogenic emission inventory under the international collaboration framework of the MICS-Asia and HTAP,  
536 *Atmospheric Chemistry and Physics*, 17, 935-963, 10.5194/acp-17-935-2017, 2017.

537 Liu, D. T., Whitehead, J., Alfara, M. R., Reyes-Villegas, E., Spracklen, D. V., Reddington, C. L., Kong, S. F., Williams, P.  
538 I., Ting, Y. C., Haslett, S., Taylor, J. W., Flynn, M. J., Morgan, W. T., McFiggans, G., Coe, H., and Allan, J. D.: Black-  
539 carbon absorption enhancement in the atmosphere determined by particle mixing state, *Nature Geoscience*, 10, 184-  
540 U132, 10.1038/ngeo2901, 2017.

541 Liu, H. K., Wang, Q. Y., Xing, L., Zhang, Y., Zhang, T., Ran, W. K., and Cao, J. J.: Measurement report: quantifying source  
542 contribution of fossil fuels and biomass-burning black carbon aerosol in the southeastern margin of the Tibetan Plateau,  
543 *Atmospheric Chemistry and Physics*, 21, 973-987, 10.5194/acp-21-973-2021, 2021.

544 Luderer, G., Trentmann, J., Winterrath, T., Textor, C., Herzog, M., Graf, H. F., and Andreae, M. O.: Modeling of biomass  
545 smoke injection into the lower stratosphere by a large forest fire (Part II): sensitivity studies, *Atmospheric Chemistry  
546 and Physics*, 6, 5261-5277, 10.5194/acp-6-5261-2006, 2006.

547 Luo, M., Liu, Y. Z., Zhu, Q. Z., Tang, Y. H., and Alam, K.: Role and Mechanisms of Black Carbon Affecting Water Vapor  
548 Transport to Tibet, *Remote Sensing*, 12, 10.3390/rs12020231, 2020.

549 Massoli, P., Onasch, T. B., Cappa, C. D., Nuamaan, I., Hakala, J., Hayden, K., Li, S. M., Sueper, D. T., Bates, T. S., Quinn,  
550 P. K., Jayne, J. T., and Worsnop, D. R.: Characterization of black carbon-containing particles from soot particle aerosol  
551 mass spectrometer measurements on the R/V Atlantis during CalNex 2010, *J Geophys Res-Atmos*, 120, 2575-2593,  
552 10.1002/2014jd022834, 2015.

553 Mätzler, C.: MATLAB functions for Mie scattering and absorption, version 2, IAP Res. Rep, 8, University of Bern, Bern,  
554 Switzerland, 2002.

555 Meehl, G. A., Arblaster, J. M., and Collins, W. D.: Effects of black carbon aerosols on the Indian monsoon, *Journal of  
556 Climate*, 21, 2869-2882, 10.1175/2007jcli1777.1, 2008.

557 Menon, S., Hansen, J., Nazarenko, L., and Luo, Y. F.: Climate effects of black carbon aerosols in China and India, *Science*,  
558 297, 2250-2253, 10.1126/science.1075159, 2002.

559 Onasch, T. B., Trimborn, A., Fortner, E. C., Jayne, J. T., Kok, G. L., Williams, L. R., Davidovits, P., and Worsnop, D. R.:  
560 Soot Particle Aerosol Mass Spectrometer: Development, Validation, and Initial Application, *Aerosol Science and  
561 Technology*, 46, 804-817, 10.1080/02786826.2012.663948, 2012.

562 Pitchford, M., Malm, W., Schichtel, B., Kumar, N., Lowenthal, D., and Hand, J.: Revised algorithm for estimating light  
563 extinction from IMPROVE particle speciation data, *Journal of the Air & Waste Management Association*, 57, 1326-  
564 1336, 10.3155/1047-3289.57.11.1326, 2007.

565 Ram, K. and Sarin, M. M.: Absorption Coefficient and Site-Specific Mass Absorption Efficiency of Elemental Carbon in  
566 Aerosols over Urban, Rural, and High-Altitude Sites in India, *Environmental Science & Technology*, 43, 8233-8239,  
567 10.1021/es9011542, 2009.

568 Ramanathan, V., Chung, C., Kim, D., Bettge, T., Buja, L., Kiehl, J. T., Washington, W. M., Fu, Q., Sikka, D. R., and Wild,  
569 M.: Atmospheric brown clouds: Impacts on South Asian climate and hydrological cycle, *P Natl Acad Sci USA*, 102,  
570 5326-5333, 10.1073/pnas.0500656102, 2005.

571 Richter, A., Burrows, J. P., Nüss, H., Granier, C., and Niemeier, U.: Increase in tropospheric nitrogen dioxide over China  
572 observed from space, *Nature*, 437, 129-132, 10.1038/nature04092, 2005.

573 Schnaiter, M., Linke, C., Möhler, O., Naumann, K. H., Saathoff, H., Wagner, R., Schurath, U., and Wehner, B.: Absorption  
574 amplification of black carbon internally mixed with secondary organic aerosol -: art. no. D19204, *J Geophys Res-  
575 Atmos*, 110, 10.1029/2005jd006046, 2005.

576 Sofiev, M., Ermakova, T., and Vankevich, R.: Evaluation of the smoke-injection height from wild-land fires using remote-  
577 sensing data, *Atmospheric Chemistry and Physics*, 12, 1995-2006, 10.5194/acp-12-1995-2012, 2012.

578 Stein, A. F., Draxler, R. R., Rolph, G. D., Stunder, B. J. B., Cohen, M. D., and Ngan, F.: NOAA'S HYSPLIT  
579 ATMOSPHERIC TRANSPORT AND DISPERSION MODELING SYSTEM, *Bulletin of the American  
580 Meteorological Society*, 96, 2059-2077, 10.1175/bams-d-14-00110.1, 2015.

581 Sun, P., Nie, W., Wang, T., Chi, X., Huang, X., Xu, Z., Zhu, C., Wang, L., Qi, X., Zhang, Q., and Ding, A.: Impact of air  
582 transport and secondary formation on haze pollution in the Yangtze River Delta: In situ online observations in Shanghai  
583 and Nanjing, *Atmos Environ*, 225, 10.1016/j.atmosenv.2020.117350, 2020.

584 Sun, P., Nie, W., Chi, X., Xie, Y., Huang, X., Xu, Z., Qi, X., Xu, Z., Wang, L., Wang, T., Zhang, Q., and Ding, A.: Two  
585 years of online measurement of fine particulate nitrate in the western Yangtze River Delta: influences of  
586 thermodynamics and N2O5 hydrolysis, *Atmospheric Chemistry and Physics*, 18, 17177-17190, 10.5194/acp-18-17177-  
587 2018, 2018.

588 Sun, Y. L., Wang, Z. F., Wild, O., Xu, W. Q., Chen, C., Fu, P. Q., Du, W., Zhou, L. B., Zhang, Q., Han, T. T., Wang, Q. Q.,  
589 Pan, X. L., Zheng, H. T., Li, J., Guo, X. F., Liu, J. G., and Worsnop, D. R.: "APEC Blue": Secondary Aerosol  
590 Reductions from Emission Controls in Beijing, *Scientific Reports*, 6, 10.1038/srep20668, 2016.

591 Tan, T. Y., Hu, M., Du, Z. F., Zhao, G., Shang, D. J., Zheng, J., Qin, Y. H., Li, M. R., Wu, Y. S., Zeng, L. M., Guo, S., and  
592 Wu, Z. J.: Measurement report: Strong light absorption induced by aged biomass burning black carbon over the  
593 southeastern Tibetan Plateau in pre-monsoon season, *Atmospheric Chemistry and Physics*, 21, 8499-8510, 10.5194/acp-  
594 21-8499-2021, 2021.

595 Ulbrich, I. M., Canagaratna, M. R., Zhang, Q., Worsnop, D. R., and Jimenez, J. L.: Interpretation of organic components  
596 from Positive Matrix Factorization of aerosol mass spectrometric data, *Atmospheric Chemistry and Physics*, 9, 2891-  
597 2918, 2009.

598 Virkkula, A.: Modeled source apportionment of black carbon particles coated with a light-scattering shell, *Atmospheric*  
599 *Measurement Techniques*, 14, 3707-3719, 10.5194/amt-14-3707-2021, 2021.

600 Wang, J., Wang, J., Cai, R., Liu, C., Jiang, J., Nie, W., Wang, J., Moteki, N., Zaveri, R. A., Huang, X., Ma, N., Chen, G.,  
601 Wang, Z., Jin, Y., Cai, J., Zhang, Y., Chi, X., Holanda, B. A., Xing, J., Liu, T., Qi, X., Wang, Q., Pohlker, C., Su, H.,  
602 Cheng, Y., Wang, S., Hao, J., Andreae, M. O., and Ding, A.: Unified theoretical framework for black carbon mixing  
603 state allows greater accuracy of climate effect estimation, *Nature communications*, 14, 2703, 10.1038/s41467-023-  
604 38330-x, 2023.

605 Wang, J. F., Ge, X. L., Chen, Y. F., Shen, Y. F., Zhang, Q., Sun, Y. L., Xu, J. Z., Ge, S., Yu, H., and Chen, M. D.: Highly  
606 time-resolved urban aerosol characteristics during springtime in Yangtze River Delta, China: insights from soot particle  
607 aerosol mass spectrometry, *Atmospheric Chemistry and Physics*, 16, 9109-9127, 2016.

608 Wang, J. F., Zhang, Q., Chen, M. D., Collier, S., Zhou, S., Ge, X. L., Xu, J. Z., Shi, J. S., Xie, C. H., Hu, J. L., Ge, S., Sun,  
609 Y. L., and Coe, H.: First Chemical Characterization of Refractory Black Carbon Aerosols and Associated Coatings over  
610 the Tibetan Plateau (4730 m a.s.l), *Environmental Science & Technology*, 51, 14072-14082, 10.1021/acs.est.7b03973,  
611 2017.

612 Wang, Q. Y., Schwarz, J. P., Cao, J. J., Gao, R. S., Fahey, D. W., Hu, T. F., Huang, R. J., Han, Y. M., and Shen, Z. X.: Black  
613 carbon aerosol characterization in a remote area of Qinghai-Tibetan Plateau, western China, *Science of the Total*  
614 *Environment*, 479, 151-158, 10.1016/j.scitotenv.2014.01.098, 2014.

615 Wang, Q. Y., Huang, R. J., Cao, J. J., Tie, X. X., Ni, H. Y., Zhou, Y. Q., Han, Y. M., Hu, T. F., Zhu, C. S., Feng, T., Li, N.,  
616 and Li, J. D.: Black carbon aerosol in winter northeastern Qinghai-Tibetan Plateau, China: the source, mixing state and  
617 optical property, *Atmospheric Chemistry and Physics*, 15, 13059-13069, 10.5194/acp-15-13059-2015, 2015.

618 Wang, Q. Y., Cao, J. J., Han, Y. M., Tian, J., Zhu, C. S., Zhang, Y. G., Zhang, N. N., Shen, Z. X., Ni, H. Y., Zhao, S. Y., and  
619 Wu, J. R.: Sources and physicochemical characteristics of black carbon aerosol from the southeastern Tibetan Plateau:  
620 internal mixing enhances light absorption, *Atmospheric Chemistry and Physics*, 18, 4639-4656, 10.5194/acp-18-4639-  
621 2018, 2018.

622 Wiedinmyer, C., Akagi, S. K., Yokelson, R. J., Emmons, L. K., Al-Saadi, J. A., Orlando, J. J., and Soja, A. J.: The Fire  
623 INventory from NCAR (FINN): a high resolution global model to estimate the emissions from open burning,  
624 *Geoscientific Model Development*, 4, 625-641, 10.5194/gmd-4-625-2011, 2011.

625 Wiedinmyer, C., Quayle, B., Geron, C., Belote, A., McKenzie, D., Zhang, X. Y., O'Neill, S., and Wynne, K. K.: Estimating  
626 emissions from fires in North America for air quality modeling, *Atmos Environ*, 40, 3419-3432,  
627 10.1016/j.atmosenv.2006.02.010, 2006.

628 Wiedinmyer, C., Kimura, Y., McDonald-Buller, E. C., Emmons, L. K., Buchholz, R. R., Tang, W. F., Seto, K., Joseph, M.  
629 B., Barsanti, K. C., Carlton, A. G., and Yokelson, R.: The Fire Inventory from NCAR version 2.5: an updated global  
630 fire emissions model for climate and chemistry applications, *Geoscientific Model Development*, 16, 3873-3891,  
631 10.5194/gmd-16-3873-2023, 2023.

632 Willis, M. D., Lee, A. K. Y., Onasch, T. B., Fortner, E. C., Williams, L. R., Lambe, A. T., Worsnop, D. R., and Abbatt, J. P.  
633 D.: Collection efficiency of the soot-particle aerosol mass spectrometer (SP-AMS) for internally mixed particulate  
634 black carbon, *Atmospheric Measurement Techniques*, 7, 4507-4516, 10.5194/amt-7-4507-2014, 2014.

635 Wu, G. X., Duan, A. M., Liu, Y. M., Mao, J. Y., Ren, R. C., Bao, Q., He, B., Liu, B. Q., and Hu, W. T.: Tibetan Plateau  
636 climate dynamics: recent research progress and outlook, *Natl Sci Rev*, 2, 100-116, 10.1093/nsr/nwu045, 2015.

637 Wu, G. X., Liu, Y. M., Wang, T. M., Wan, R. J., Liu, X., Li, W. P., Wang, Z. Z., Zhang, Q., Duan, A. M., and Liang, X. Y.:  
638 The influence of mechanical and thermal forcing by the Tibetan Plateau on Asian climate, *Journal of*  
639 *Hydrometeorology*, 8, 770-789, 10.1175/jhm609.1, 2007.

640 Xu, B. Q., Cao, J. J., Hansen, J., Yao, T. D., Joswia, D. R., Wang, N. L., Wu, G. J., Wang, M., Zhao, H. B., Yang, W., Liu,  
641 X. Q., and He, J. Q.: Black soot and the survival of Tibetan glaciers, *P Natl Acad Sci USA*, 106, 22114-22118,  
642 10.1073/pnas.0910444106, 2009.

643 Xu, J. Z., Zhang, Q., Shi, J. S., Ge, X. L., Xie, C. H., Wang, J. F., Kang, S. C., Zhang, R. X., and Wang, Y. H.: Chemical  
644 characteristics of submicron particles at the central Tibetan Plateau: insights from aerosol mass spectrometry,  
645 *Atmospheric Chemistry and Physics*, 18, 427-443, 10.5194/acp-18-427-2018, 2018.

646 Yang, J. H., Kang, S. C., Chen, D. L., Zhao, L., Ji, Z. M., Duan, K. Q., Deng, H. J., Tripathee, L., Du, W. T., Rai, M., Yan,  
647 F. P., Li, Y., and Gillies, R. R.: South Asian black carbon is threatening the water sustainability of the Asian Water  
648 Tower, *Nature Communications*, 13, 10.1038/s41467-022-35128-1, 2022.

649 Yang, K., Wu, H., Qin, J., Lin, C. G., Tang, W. J., and Chen, Y. Y.: Recent climate changes over the Tibetan Plateau and  
650 their impacts on energy and water cycle: A review, *Global and Planetary Change*, 112, 79-91,  
651 10.1016/j.gloplacha.2013.12.001, 2014.

652 Yao, T., Thompson, L., Mosbrugger, V., Zhang, F., Ma, Y., Luo, T., Xu, B., Yang, X., Joswiak, D. R., Wang, W., Joswiak,  
653 M. E., Devkota, L. P., Tayal, S., Jilani, R., and Fayziev, R.: Third Pole Environment (TPE), *Environ. Dev.*, 3, 52-64,  
654 <https://doi.org/10.1016/j.envdev.2012.04.002>, 2012a.

655 Yao, T. D., Thompson, L., Yang, W., Yu, W. S., Gao, Y., Guo, X. J., Yang, X. X., Duan, K. Q., Zhao, H. B., Xu, B. Q., Pu,  
656 J. C., Lu, A. X., Xiang, Y., Kattel, D. B., and Joswiak, D.: Different glacier status with atmospheric circulations in  
657 Tibetan Plateau and surroundings, *Nature Climate Change*, 2, 663-667, 10.1038/nclimate1580, 2012b.

658 Yuan, Q., Xu, J. Z., Wang, Y. Y., Zhang, X. H., Pang, Y. E., Liu, L., Bi, L., Kang, S. C., and Li, W. J.: Mixing State and  
659 Fractal Dimension of Soot Particles at a Remote Site in the Southeastern Tibetan Plateau, *Environmental Science &  
660 Technology*, 53, 8227-8234, 10.1021/acs.est.9b01917, 2019.

661 Zhang, M. X., Zhao, C., Cong, Z. Y., Du, Q. Y., Xu, M. Y., Chen, Y., Chen, M., Li, R., Fu, Y. F., Zhong, L., Kang, S. C.,  
662 Zhao, D. L., and Yang, Y.: Impact of topography on black carbon transport to the southern Tibetan Plateau during the  
663 pre-monsoon season and its climatic implication, *Atmospheric Chemistry and Physics*, 20, 5923-5943, 10.5194/acp-20-  
664 5923-2020, 2020.

665 Zhang, Q., Worsnop, D. R., Canagaratna, M. R., and Jimenez, J. L.: Hydrocarbon-like and oxygenated organic aerosols in  
666 Pittsburgh: insights into sources and processes of organic aerosols, *Atmospheric Chemistry and Physics*, 5, 3289-3311,  
667 10.5194/acp-5-3289-2005, 2005a.

668 Zhang, Q., Alfarra, M. R., Worsnop, D. R., Allan, J. D., Coe, H., Canagaratna, M. R., and Jimenez, J. L.: Deconvolution and  
669 quantification of hydrocarbon-like and oxygenated organic aerosols based on aerosol mass spectrometry,  
670 *Environmental Science & Technology*, 39, 4938-4952, 10.1021/es048568l, 2005b.

671 Zhang, Q., Jimenez, J. L., Canagaratna, M. R., Ulbrich, I. M., Ng, N. L., Worsnop, D. R., and Sun, Y. L.: Understanding  
672 atmospheric organic aerosols via factor analysis of aerosol mass spectrometry: a review, *Anal Bioanal Chem*, 401,  
673 3045-3067, 2011.

674 Zhang, R., Wang, H., Qian, Y., Rasch, P. J., Easter, R. C., Ma, P. L., Singh, B., Huang, J., and Fu, Q.: Quantifying sources,  
675 transport, deposition, and radiative forcing of black carbon over the Himalayas and Tibetan Plateau, *Atmospheric  
676 Chemistry and Physics*, 15, 6205-6223, 10.5194/acp-15-6205-2015, 2015.

677 Zhang, X. H., Xu, J. Z., Kang, S. C., Liu, Y. M., and Zhang, Q.: Chemical characterization of long-range transport biomass  
678 burning emissions to the Himalayas: insights from high-resolution aerosol mass spectrometry, *Atmospheric Chemistry  
679 and Physics*, 18, 4617-4638, 10.5194/acp-18-4617-2018, 2018.

680 Zhao, D. F., Schmitt, S. H., Wang, M. J., Acir, I. H., Tillmann, R., Tan, Z. F., Novelli, A., Fuchs, H., Pullinen, I., Wegener,  
681 R., Rohrer, F., Wildt, J., Kiendler-Scharr, A., Wahner, A., and Mentel, T. F.: Effects of NO<sub>x</sub> and SO<sub>2</sub> on the secondary  
682 organic aerosol formation from photooxidation of  $\alpha$ -pinene and limonene, *Atmospheric Chemistry and Physics*, 18,  
683 1611-1628, 10.5194/acp-18-1611-2018, 2018.

684 Zhao, Z. Z., Cao, J. J., Shen, Z. X., Xu, B. Q., Zhu, C. S., Chen, L. W. A., Su, X. L., Liu, S. X., Han, Y. M., Wang, G. H.,  
685 and Ho, K. F.: Aerosol particles at a high-altitude site on the Southeast Tibetan Plateau, China: Implications for  
686 pollution transport from South Asia, *J Geophys Res-Atmos*, 118, 11360-11375, 10.1002/jgrd.50599, 2013.

687 Zhao, Z. Z., Wang, Q. Y., Xu, B. Q., Shen, Z. X., Huang, R. J., Zhu, C. S., Su, X. L., Zhao, S. Y., Long, X., Liu, S. X., and  
688 Cao, J. J.: Black carbon aerosol and its radiative impact at a high-altitude remote site on the southeastern Tibet Plateau,  
689 *J Geophys Res-Atmos*, 122, 5515-5530, 10.1002/2016jd026032, 2017.



690 Zheng, G. J., Sedlacek, A. J., Aiken, A. C., Feng, Y., Watson, T. B., Raveh-Rubin, S., Uin, J., Lewis, E. R., and Wang, J.:  
691 Long-range transported North American wildfire aerosols observed in marine boundary layer of eastern North Atlantic,  
692 Environment International, 139, 10.1016/j.envint.2020.105680, 2020.

693 Zhou, W., Wang, Q. Q., Zhao, X. J., Xu, W. Q., Chen, C., Du, W., Zhao, J., Canonaco, F., Prévôt, A. S. H., Fu, P. Q., Wang,  
694 Z. F., Worsnop, D. R., and Sun, Y. L.: Characterization and source apportionment of organic aerosol at 260 m on a  
695 meteorological tower in Beijing, China, Atmospheric Chemistry and Physics, 18, 3951-3968, 10.5194/acp-18-3951-  
696 2018, 2018.

697 Zhu, C. S., Cao, J. J., Hu, T. F., Shen, Z. X., Tie, X. X., Huang, H., Wang, Q. Y., Huang, R. J., Zhao, Z. Z., Mocnik, G., and  
698 Hansen, A. D. A.: Spectral dependence of aerosol light absorption at an urban and a remote site over the Tibetan  
699 Plateau, Sci Total Environ, 590, 14-21, 10.1016/j.scitotenv.2017.03.057, 2017.

700 Zhu, C. S., Cao, J. J., Xu, B. Q., Huang, R. J., Wang, P., Ho, K. F., Shen, Z. X., Liu, S. X., Han, Y. M., Tie, X. X., Zhao, Z.  
701 Z., and Chen, L. W. A.: Black Carbon Aerosols at Mt. Muztagh Ata, a High-Altitude Location in the Western Tibetan  
702 Plateau, Aerosol and Air Quality Research, 16, 752-763, 10.4209/aaqr.2015.04.0255, 2016.

703